Design Optimization of the ITER In-Vessel Plasma-Position Reflectometry System Antenna

Nicolau José Moreno Velez

Thesis to obtain the Master of Science Degree in

Aerospace Engineering

Supervisor(s): Prof. Miguel António Lopes de Matos Neves
Dr. Hugo Filipe Diniz Policarpo

Examination Committee

Chairperson: Prof. Fernando José Parracho Lau
Supervisor: Prof. Miguel António Lopes de Matos Neves
Member of the Committee: Prof. José Viriato Araújo dos Santos

November 2016

Dedicated to someone special...

Acknowledgments

After concluding this work, I would like to express my gratitude to:

My supervisor, Professor Miguel de Matos Neves, for his permanent availability to help me, for his invaluable advices and guidance not only throughout all the time I worked on this thesis, but also as his student.

My co-supervisor, Professor Hugo Policarpo, for all his time and effort spent on me, for his support and motivation along this work, for the trust he placed in me, always always taking into account my suggestions along this project and for granting me the scholarship that made this work possible.

Paulo Quental for his warm welcome when I arrived at IPFN, for his extremely helpful advices, guidance and his continuous availability to help me throughout all of this work.

Instituto de Plasmas e Fusão Nuclear, for all the conditions provided, the trust put on me and for the opportunity of working in this project.

Everyone at Instituto de Plasmas e Fusão Nuclear, for all their help and support during this project.

My scholarship colleagues Fábio Costa and Diogo Murteira for their help, support and motivation during this work.

My friends Sérgio and Mafalda for their constant support and incentive along this path, for their company and motivation.

To everyone I met along this path, that somehow helped, motivated and inspired my to keep going. To my family, specially to my parents and my sister, for their unconditional support and motivation.

To Marta, for her endless support and motivation, for her valuable advices and companion along all these years.

The work leading to this publication has received financial support from Fundação para a Ciência e Tecnologia (FCT) through project UID/FIS/50010/2013 through grant BL 54/2016. Author further acknowledge the data provided by Fusion for Energy under F4E-FPA-375-04.

Resumo

Este trabalho apresenta um estudo de análise estrutural termoelástica e desenvolvimento de um design óptimo para a antena pertencente ao ITER PPR, utilizando análises termo-estruturais de FE implementadas no programa comercial ANSYS. Assim, é desenvolvida uma metodologia bi-direccional de CAD-FE, são realizados alguns estudos paraméricos e é utilizada a metodologia de optimização topológica SIMP, tal como os algoritmos ASO e AMO. Os parâmetros considerados são as dimensões da cobertura de material adicional para minimizar as temperaturas e deslocamentos máximos da antena. Inicialmente, um estudo paramétrico sobre a temperatura e deslocamentos máximos obtidos na antena é realizado para determinar o intervalo de optimização de interesse. Seguidamente, os métodos de optimização ASO e AMO são utilizados nestes intervalos para encontrar distribuições de material optimizadas na antena. Os modelos obtidos apresentam máximos mais baixos da temperatura máxima registada ao longo da antena (10%), temperaturas médias mais baixas (10%) e deslocamentos máximos mais baixos ao longo da antena (18%). Neste estudo, os resultados obtidos com optimização topológica tendem a remover a maioria do material nas áreas de concepção, que é um efeito conhecido. A cobertura adicional em praticamente todo o comprimento da antena é capaz de reduzir a temperatura e deslocamentos máximos, sendo uma contribuição para o seu design. Um dos importantes aspectos a ter em consideração é a definição de uma forma de confirmar, sem testes experimentais, a súbita mudança observada na resposta estrutural da antena quando sujeita a radiação de calor e ao seu próprio peso nas condições analisadas.

Palavras-chave: ITER, antena de PPR, Optimização, Minimização de Temperatura, Minimização de Deformação

Abstract

This dissertation presents a study focused on thermoelastic structural analysis and development of an optimized design for the ITER in-vessel PPR antenna using thermal-structural finite element (FE) analysis implemented in the commercial FE program ANSYS. For it, a two-way parameterized CAD-FE methodology is developed, some parametric studies performed, and the SIMP topology optimization and ASO and AMO algorithms are used. The parameters considered are the dimensions of additional material coverage to minimize the maximum temperatures and displacements of the antenna. Initially, a parametric study regarding the maximum temperature and displacement achieved in the antenna is performed to establish the optimization interval of interest. Afterwards, optimization methods ASO and AMO are used in these intervals to find optimized material distributions in the antenna. The optimized designs obtained present both lower maximums in the achieved maximum temperature along the antenna (10%) as well as for average temperatures (10%) and maximum displacement along the antenna (18%). In this particular case, the results obtained with topology optimization tend to remove most of the material in the design areas which is a known effect. An achieved contribution to the antenna design, is that additional coverage in thickness in practically all the length is able to reduce the maximum temperature and displacement. One of the most important aspects to consider is to set a way to confirm, if possible without experimental test, the sudden change observed in the structural response of the antenna when subject to heat radiation and its self-weight in the conditions here analyzed.

Keywords: ITER, PPR antenna, Optimization, Temperature Minimization, Displacement Minimization

Contents

List of Tables

List of Figures

Nomenclature

AMO Adaptive Multiple Objective.

ASO Adaptive Single Objective.

CAD Computer Aided Design.

CTS Collective Thomson Scattering.

$ECRH$ IElectron Cyclotron Resonance Heating

$Eq.$ Equation.

FE Finite Elements.

FEA Finite Element Analysis.

FEM Finite Element Method.

$Fig.$ Figure.

LHS Latin Hypercube Sampling.

$MINLP$ Mixed-Integer Non-Linear Programming.

$MISQP$ Mixed-Integer Sequential Quadratic Programming.

$MOGA$ Multi Objective Genetic Algorithm.

OSF Optimal Space-Filling Design.

PPR ANSYS® Plasma Position Reflectometry.

$SIMP$ Solid Isotropic Material with Penalization.

SO Shape Optimization.

SQP Sequential Quadratic Programming.

TO Topology Optimization.

Greek symbols

α Thermal expansion coefficient.

Δ Variation of a parameter.

λ Wavelength.

λ_{abs} Absorbed radiation.

λ_{tr} Transmitted radiation.

$\prod$ Total potential energy.

ρ Material density.

ρ_a Atomic density.

ρ_g Mass density.

ρ_{ref} Reflected radiation.

σ Stress.

σ^t Thermal stress.

σ_s Stefan-Boltzmann's constant.

θ_i, θ_j Angles between the surfaces normal vectors and the dashed line uniting the areas centroids in view factor.

ε^θ Elastic strain.

ε^t Thermal strain.

ε_{em} Emissivity.

Transmitted radiation.

Roman symbols

A Area.

A_i, A_j Area of element i or j.

C Elastic strain energy.

c Heat capacity.

E_b Blackbody emissive power.

E_m Emitted radiation.

E_p Particle energy.

E_{el} Elastic properties.

F_n Factor between the reference surface and each of the target pixels.

F_{ij}, F_{ji} View factor between surfaces i and j.

G Irradiation.

G_{ref} Reflected radiation.

G_{transm} Transmitted radiation.

$H(E_p)$ Heating response.

H_{conv} Global convection.

H_{rad} Global radiation.

J Radiosity of a surface.

J_i, J_j Radiosity of elements i and j.

k Thermal conductivity coefficient.

K_K Global conductivity.

K_T General global conductivity.

M_j Normalized objective for output parameter in AMO.

N_i Normalized objective for input parameter in AMO.

p^S Surface pressures.

p^V Body forces.

Q Internal heat generation.

q Heat flux.

q_r incoming heat flow per unit area.

R_B Global heat flux.

R_h Global convection.

R_Q Global heat generation.

R_T General global thermal load.

R_{cond} Thermal resistance in conduction.

R_{hrad} .

R_{ij} Direct length between the centroid points of the two surfaces.

S_1 Boundary condition one.

S_4 Boundary condition four.

T	Temperature.
t	Time.
T_i, T_j	Temperature of elements i and j.
T_s	Specified temperature.
u	Displacement.
V	Volume.
w_i	Weight of input parameter in AMO.
w_j	Weight of output parameter in AMO.
x, y, z	Directions.
Y	Body's cross section.
p	Pressure.
T_0	Initial temperature.
T_f	Final temperature.

Subscripts

i, j, k	Computational indexes.
n	Normal component.
ref	Reference condition.
x, y, z	Cartesian components.

Chapter 1

Introduction

The present thesis approaches the matter of structural optimization of the Plasma Position Reflectometry (PPR) system antenna that measures the edge electron density profile of the plasma, providing real-time supplementary contribution to the magnetic measurements of the plasma-wall distance in the International Thermonuclear Experimental Reactor (ITER). This is a nuclear fusion reactor project, which is meant to build the world's largest Tokamak in order to provide great amounts of fusion energy, to study and to test the evolution of the future fusion power plants.

The system being studied in this thesis is located in the tokamak's core, which is subjected to an extremely high amount of thermal and neutronic radiation loads, while immersed in a vacuum environment, which will lead to considerable thermal expansions and tensions. This phenomena needs to be minimized as these structure body changes can actually adulterate the antenna's purposes not to mention that it can lead to clashes with the surrounding components, possibly resulting in the failure of the system. Hence, high stresses may lead to the plastic deformation of the material and high temperatures may lead to material phase changes and consequent loss of the antenna's subservience.

The main objective of this thesis is to investigate how the problems stated above (high temperature, displacement, stress) may be minimized through structural optimization of the PPR antenna. In order to achieve this, a process of refining the antenna's design using optimization methodologies, namely Single or Multiple Objective Parametric Optimization and Topology Optimization (TO), is here explored.

Single or multiple objective parametric optimization are methods in which parameters belonging to a given structure's design are chosen and then changed in their values in order to find the best answer given an objective function. This can occur when only one objective (single) is defined or when two or more objectives (multiple) are defined, allowing more than one problem to be solved, while respecting the desired relationship between them.

Topology optimization method is also considered in this study. It aims at relieving a determined structure's weight without undervaluing its purpose and capability to hold a certain kind and amount of structural loads. This method is able to increase the structure stiffness while reducing its volume through the minimization of the elastic strain energy of the body. It is part of the planning of many components inherent to a great amount of structures that surround us, such as infrastructures [1], industrial machinery

[2] and transportation [3].

Many authors have referred to this method, and many studies have been conducted in this matter, which was more significantly approached by Bendsøe and Kikuchi [4] and substantial information can be seen in Sigmund [5] and, in a more embracing way in [6]. These authors were responsible for introducing this kind of structural optimization, giving way for the creation of new and improved methods.

1.1 Motivation

In engineering, the pursuit for something stronger, lighter, the pursuit for efficiency, for knowledge, for innovation, for something better, will always be present. It is based on these ideas that technology enhancement builds its pillars and it is based on these pillars that we are allowed to dream the world of tomorrow.

When looking towards a project, and talking about an aerospace project, it's not easy to decide how we can improve an idea of that size and complexity. So, while analysing it from one edge to another, we must pay attention not only on the main features, but also on the small ones. When talking about aerospace structures, it is of extreme importance to have in mind that grams can translate into great amounts of fuel losses, which can put the viability of the project at risk. Knowing how to maintain a component's functionality while diminishing its weight is a very powerful tool that can lead to great economical and structural savings.

There are in literature description of components of aircrafts being manufactured from this kind of optimization, where the main goal is to have the less material as possible in order to fulfil all the structural requirements. This method is being used by main aeronautic companies to work their way up to lighter airplanes, where key elements like pylons (whether to hold the engines or even to hold bellic material), or even leading edge ribs (from Airbus A380 [7] Fig.1.1(b)) have been successfully built upon the application of topology optimization.

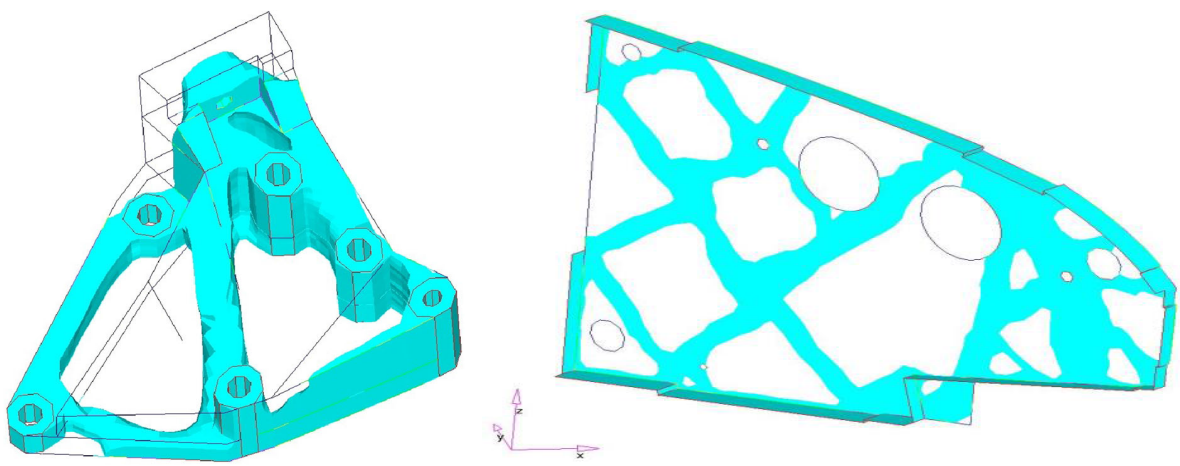

(a) Topolgy Optimized Engine Bracket [8]

(b) Topology Optimized Leading Edge Rib [7]

Figure 1.1: Topology Optimization applied in aircraft components

Although it is still a relatively recent field (with less than thirty years), TO is already being used in further studies and experiments regarding aerospace engineering, not only serving as a tool to optimize small details like engine brackets [8](Fig.1.1(a)) or door hinges [9], but also to optimize greater components as the front fuselage of an aircraft [10], as aircraft pylons [11] or even studies performed in non-conventional aircrafts wings [12].

Given the fact that already many aeronautical parts and structures are already being used in aircrafts but also looking at the results of the studies performed, it may be claimed that TO is already a very useful tool to the Aerospace field and one can only expect that its application keeps growing in a near future.

Another existing bridge between this work and the Aerospace field is related to the environment in which the components being studied and the satellites placed in Earth Orbit are located. Identically to the conditions experienced in space, also the in-vessel components are immersed in a vacuum environment, once these are located inside a vacuum chamber. Besides this, the nuclear fusion process that occurs in the sun also occurs inside the nuclear fusion reactor. This process releases high amounts of energy which can be of thermal or ionizing nature, even though the energy released in the sun is of higher proportions. The radiation inflicts the satellites through heat transfer by radiation and identically, in the reactor, inflicts the components also through radiation process. By this, high temperatures are achieved in the components hit by the thermal and ionizing radiation, making a study in this matter of high interest in both cases.

1.2 ITER

ITER is a worldwide green energy project that involves thirty five nations in the construction of a giant magnetic fusion equipment that is called Tokamak. This device is going to be the biggest in the world of its kind and the members of ITER (China, the European Union, India, Japan, Korea, Russia and the United States) are now committed in a 35-year cooperation to build and implement a experimental design in Saint Paul-lez-Durance, France.

In Fig.1.2, the Tokamak components are illustrated and they are divided in five main groups, each with its own constituents components: Divertor, Cryostat, Magnets, Vacuum Vessel and Blankets.

The divertor group is responsible for the extraction of heat and ash generated by the fusion reaction, while minimizing plasma contamination and protecting the surrounding elements from the generated loads. Many of the components in the divertor also play an important role in diagnostics regarding physics evaluation and optimization and plasma control.

Concerning the cryostat, this is a giant high-vacuum pressure chamber (the largest ever built, 3.85×10^6 kg) that is responsible for the supply of high vacuum and super-cool environment for the vacuum vessel and the superconducting magnets. As for other sections in the tokamak, the cryostat will have maintenance accesses that allow not only technicians to travel through but also parts and auxiliary systems like cooling or heating.

ITER's magnet system will also be of great proportions (1×10^7 Kg) and will be responsible for the production of the magnetic fields that will initiate, confine, shape and control the plasma. With

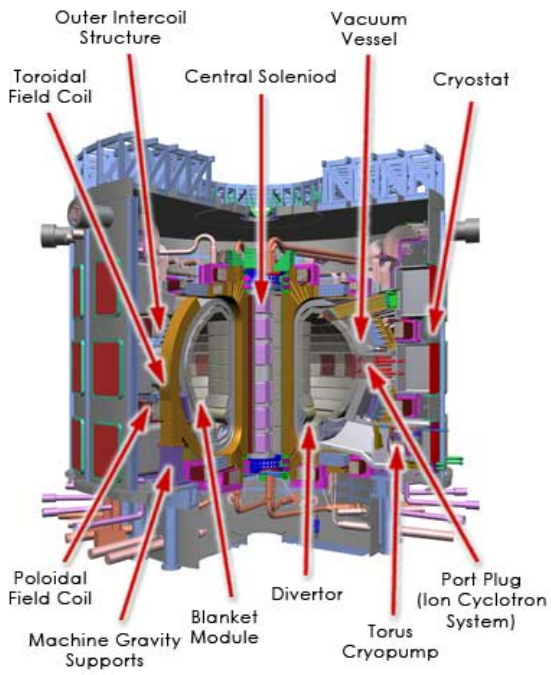

Figure 1.2: Cutaway of the ITER Tokamak with the main components ilustrated [13]

the objective of becoming superconducting magnets, which are able to carry higher current, produce stronger magnetic field than conventional counterparts and are also less power consumers and cheaper to operate, a temperature of -269°C) has to be achieved. Besides this, the magnet system is divided in six main subsystems [14]:

- Toroidal Field System - composed by eighteen D-shaped toroidal field magnets, this system has the task of producing a magnetic field in order to confine the plasma particles;
- Poloidal Field System - composed by six ring-shaped poloidal field coils, this system has the mission of shaping the plasma and keeping it away from the walls, increasing its stability;
- Central Solenoid - considered the main girder in the magnet system, the solenoid allows a powerful current to be induced in the plasma and maintained during long plasma pulses;
- Correction Coils - composed by eighteen superconducting correction coils, this system will compensate for field errors caused by geometrical deviations due to manufacturing and assembly tolerances;
- Magnet Feeders - composed by thirty one superconducting feeders, with these having the task of conveying and regulating the cryogenic liquids to cool and control the temperature of the magnets and connecting the magnets to their power supplies;
- In-Vessel Coils - composed by two main non-superconducting coil systems, where two coils will be responsible for vertical stabilization of the plasma, the remaining twenty seven coils (Edge-Localized Modes) will create resonant magnetic perturbations in the plasma so that certain instabilities are avoided.

The vacuum vessel is a hermetically sealed container where the experiments will occur. Besides this, the vacuum vessel provides a high-vacuum environment for the plasma, improves radiation shielding and plasma stability, acts as the primary confinement barrier for radioactivity, and provides support for in-vessel components such as the blanket and the divertor. As for the cryostat, this system also possesses openings for diagnostics and heating and systems, as for remote handlings.

The blankets system, which is composed by four hundred and forty blanket modules covering the inner walls of the vacuum vessel, protect the steel structure and the superconducting toroidal field magnets from the heat and high-energy neutrons produced by the fusion reactions. The clash of neutrons with the blankets makes a part of their kinetic energy to be transferred in the form of heat that will be collected by the water coolant system [14]. The energy collected will be used for electrical power production. In addition to the already mentioned purposes of the blankets, they're useful to protect diagnostic systems and plasma heating systems.

1.3 PPR System

The ITER PPR System [15] will be used to provide real-time estimates of the distance between the position of the magnetic separatrix and the first-wall at four pre-defined locations also known as gaps 3, 4, 5, and 6, complementing the information provided by the magnetic diagnostics. This is a mechanism that launches/receives a signal in the range between 15 and 75 GHz to estimate the distance between the plasma and the first wall.

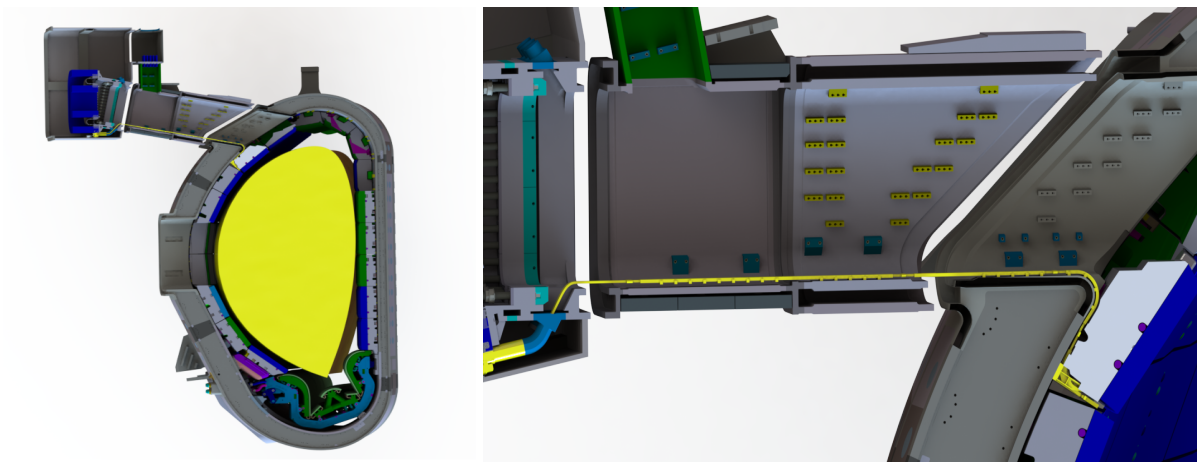

(a) Global PPR System (b) GAP 4 of the PPR System

Figure 1.3: ITER PPR System

In Fig.1.3(a) it is possible to see the global PPR system, where the plasma (yellow colored) is illustrated, as well as the remaining components and the magnified GAP 4 in Fig. 1.3(b), which is where the antenna being studied is located. Given the fact that the antenna is in direct sight of the plasma, as it is located between two blanket modules, it is considered a critical component from a structural integrity point of view.

In Fig.1.4 are illustrated the most relevant components considered in this thesis, where one can see

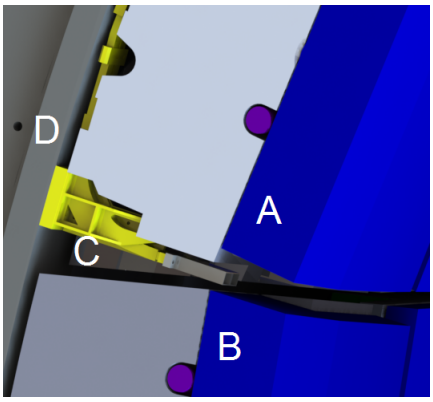

Figure 1.4: CAD model of PPR in-vessel components: A - upper blanket module, B - lower blanket module, C - PPR in-vessel components and D - vacuum vessel.

the gap in which plasma radiation, neutronics loads, and stray-radiation from Electron Cyclotron Resonance Heating (ECRH) and Collective Thomson Scattering (CTS) will pass through inflicting the antenna directly. As seen in [16], all these loads will cause extremely high temperatures on the component, that will lead to consequent deformations. These events can compromise the data that is going to be retrieved by the antenna, as well as the well being of the model and this is why the optimization of this part is of such high importance.

1.4 Contents Overview

The present document is divided in five main chapters, where the first is the Introduction. This initial chapter contains a brief description of what are the main questions, as well as its objectives and motivation.

In the chapter 2 a theoretical background of all the subjects that are involved in this paper are synthetized. Initially, a description of the structures being studied as well as their environment (fusion reactor and ITER) is presented. Proceeding this, the Finite Elements (FE) models and equations of the thermoelasticity problems, as well as the Radiation problem are introduced. To conclude, an introduction to the different types of structural optimization methodologies are presented, culminating with a brief introduction to TO and its application to thermoelasticity problems.

In chapter 3 the methodologies applied in this work are described. Namely the Computer Aided Design (CAD) model development, the integration of the CAD model in the FEM software as well as the Finite Element Method (FEM) solvers being used, the parametric studies and the TO methods.

In chapter 4 are presented the results. Starting from the first approach to the problem, where a parametric study is performed in a simplified model to investigate what would the structure behaviour under similar circumstances. Hereafter, a ”validation” and verification step is presented in order to validate the topology optimization software used, where computational results are presented and verified to previous academic works. After this, a brief description of the targets of the optimization are established, followed by the sensitivity parametric results, that defines the optimization regions. Following, the optimization results and a brief discussion are presented for each target and objective.

To conclude, in the chapter 5, a list of the main findings in the present work, either in results as in difficulties encountered along the work, are presented. In addition to this, the ideas/topics to be addressed in the future are also referred.

Chapter 2

Fundamentals

In this chapter, the theoretical fundaments that support the work developed are presented in a brief manner. Hence, thermoelasticity, heat transfer processes, FEM and the optimization processes are presented next.

2.1 Thermoelasticity Problem

An isotropic body that is subjected to a temperature higher than its equilibrium temperature T_0, is likely to suffer body deformations by means of thermal expansion. This temperature difference $\Delta T = T_f - T_0$ where T_f is the new temperature imposed in the body, will generate thermal stresses and thermal strains which considering Hooke's law can be expressed as:

$$\{\sigma\} = [E]\{\varepsilon^e\} \tag{2.1}$$

Where $[E]$ is the Elastic properties matrix, $\{\sigma\} = \{\sigma_x \ \sigma_y \ \sigma_z \ \tau_{xy} \ \tau_{xz} \ \tau_{yz}\}$ the stress vector and $\{\varepsilon^e\}$ is the elastic strain vector for small deformations expressed as:

$$\{\varepsilon^e\} = \{\varepsilon\} - \{\varepsilon^t\} \tag{2.2}$$

where $\{\varepsilon^t\} = \{\alpha T \ \alpha T \ \alpha T \ 0 \ 0 \ 0\}$. Looking at the composition of the thermal strain $\{\varepsilon^t\}$, where α is the thermal expansion coefficient, it is possible to verify that the temperature imposed will not affect the shear strains once these are equal to 0.

From Eq. 2.1 and Eq. 2.2 and assuming that both $[E]$ and α remain constant along the heating process, one obtains:

$$\{\sigma^t\} = [E]\{\varepsilon^t\} \tag{2.3}$$

where $\{\sigma^t\}$ is the thermal stresses vector.

2.2 Thermal Problem

One of the most critical parts of the study is to perform a thermal analysis on the antenna in order to infer what will be the resulting temperature distribution along the model and what changes will it cause. Once it is of major importance to the work being developed, a brief introduction will be given to the matter of heat transfer. There are three defined types of heat transfer, where each can be dependent or not of the medium where the phenomena will occur:

- Convection – Type of heat transfer where energy will be given to the surrounding fluid and/or gas of the heat generating body;

- Conduction – Type of heat transfer where energy will be transferred to the atoms present in a material/solid medium;

- Radiation – Type of heat transfer where energy is transferred in electromagnetic form, making it possible to occur even if no matter (solid or fluid/gas) is involved.

As mentioned in section 1, our model is immersed in a vacuum environment, which makes heat transfer by convection impossible to exist. By that, only the two remaining processes will be further developed in this section.

2.2.0.1 Conduction

Conduction takes place in a solid material in between points that are at different temperatures. This will cause a necessity for thermal balance, where the atoms present in the points with the higher temperature will provide energy to their surrounding atoms through collision. Imagine a plane rectangular wall, with a constant cross-sectional area. If one edge is at a higher temperature than the opposite one, a heat flux (here assumed in a one-dimensional heat conduction process) will be generated, which can be explained by Fourier's Law:

$$q = -\frac{kA}{\Delta x}(\Delta T) \tag{2.4}$$

with k being the thermal conductivity of the material/solid, A the cross-sectional area, ΔT the temperature difference between the two surfaces and Δx the wall length. The thermal resistance in conduction can be associated with the previous in the following way:

$$R_{cond} = \frac{\Delta x}{kA} \tag{2.5}$$

which leads to the rearranging of Eq. 2.4 in the following way:

$$q = -\frac{\Delta T}{R_{cond}} \tag{2.6}$$

2.2.0.2 Radiation

It is through radiation that most of the energy travels in our universe. Whether is light emitted by stars and reflected by other celestial bodies, radiation that powers not only our satellites orbiting Earth but also all the things we know and depend on, it is through radiation that all life as we know it is able to subsist.

Every body that has a temperature greater than 0 is able to emit and absorb radiation in different wavelengths in its spectrum; a great example of this is our own bodies, which are constantly emitting and absorbing radiation.

A particular case of radiation is the so called blackbody. This is a case where an idealized body absorbs all incident electromagnetic radiation regardless of frequency and incidence ,i.e., there is no surface that can emit more nor absorb more than a blackbody surface, with its emissivity will behave independently from the radiation direction (diffuse), while its absorptivity behaves independently from wavelength (λ) or temperature (T).

$$E_b = \sigma_s T^4 \tag{2.7}$$

As seen in Eq. 2.7, known as the Stefan–Boltzmann equation, the intensity of the blackbody total emissive power will oscillate directly with the temperature to the fourth power, with T [K] being the body temperature and $\sigma_s[Wm^{-2}K^{-4}]$ the constant of proportionality or more commonly known, the Stefan–Boltzmann constant. However, this is only a theoretical case, in reality no surface can behave as a blackbody, i.e., no body has an emissivity of 1 nor an absorptivity of 1, which leads to an adjustment in the previous equation:

$$E = \sigma_s \varepsilon_{em} T^4 \tag{2.8}$$

In Eq. 2.8, the emissivity parameter was added and it can adopt a range of values from 0 to 1, with 1 meaning that the surface behaves like a blackbody surface. This parameter can be expressed as a value determined by the ratio of emissivity power of the surface being studied and the emissivity power of a blackbody surface:

$$\varepsilon_{em} = \frac{E}{E_b} \tag{2.9}$$

Now regarding the case where radiation reaches another surface, creating a process named irradiation (G). As previously mentioned, blackbody surfaces do not exist and as a result, not only the emissivity will not be 1, as also the absorptivity will not be 1. This effect means that the incident radiation won't be totally absorbed but otherwise divided into three different outcomes where part of this radiation may be reflected (ρ_{ref} or G_{ref}), another part may be transmitted (τ) and the last part may be absorbed (λ_{abs}). These three portions of radiation obey a simple rule (conservation of energy) in which each varies from 0 to 1:

$$\rho_{ref} + \tau + \lambda_{abs} = 1 \tag{2.10}$$

Another concept is the energetic radiosity of a surface (J), which consists in a the sum of the emitted radiation (E_{em}) with the reflected radiation:

$$J(\lambda, T) = E_{em} + G_{ref} + G_{transm} \tag{2.11}$$

where G_{ref} is the reflected radiation and G_{transm} is the transmitted radiosity which vanishes for opaque surfaces. Now, replacing the above equation with Eq. 2.8, the results obtained are:

$$J(\lambda, T) = \varepsilon(\lambda, T)\sigma T^4 + \rho_{ref}(\lambda, T)G \tag{2.12}$$

where $\rho(\lambda, T)G$ represents the portion (ρ) of radiosity G that is reflected ($\rho G = G_{ref}$). However, the amount of radiation that reaches another surface will be conditioned by the way this surface is disposed towards the emitter one, i.e., only a given amount of the radiation emitted by a surface i will reach the receiver surface j. This quantity of radiation can be measured by the view factor F_{ij}, which is an adimentional value that ranges between 0 and 1 but for more complex cases where a greater number of surfaces (N) is present and assuming that both surface areas are the same, the following equation can be applied:

$$\sum_{j=1}^{N} F_{ij} = 1 \tag{2.13}$$

Eq. 2.13 is a simplified case of the generic expression for two distinct surface areas A_i and A_j radiation exchange, where the view factor is given by:

$$F_{ij} = \frac{1}{A_i} \int_{A_i} \int_{A_j} \frac{cos(\theta_i)cos(\theta_j)}{\pi R_{ij}^2} dA_i dA_j \tag{2.14}$$

and, looking at fig. 2.1, R_{ij} is the direct length between the centroid points of the two surfaces and θ_i and θ_j are the angles between the surfaces normal vectors and the dashed line uniting the areas centroids.

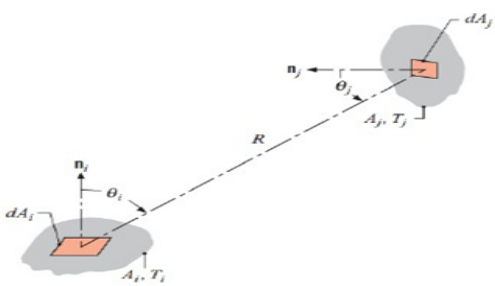

Figure 2.1: View factor between elemental surfaces dA_i and dA_j in [17]

For calculation purposes, a very useful property of this mechanism is its reciprocity, which allows us

to find the opposite view factor if the original is already know (and vice versa) as follows:

$$F_{ji} = \frac{A_i F_{ij}}{A_j} \tag{2.15}$$

As mentioned previously in this section, not all the radiation emitted by a surface will reach another one. An illustration of this phenomena is presented through the concept of radiation network in Fig. 2.2, where E_{bi} represents the emitter blackbody and the posterior resistance reflects the fact that $\varepsilon <$ 1,

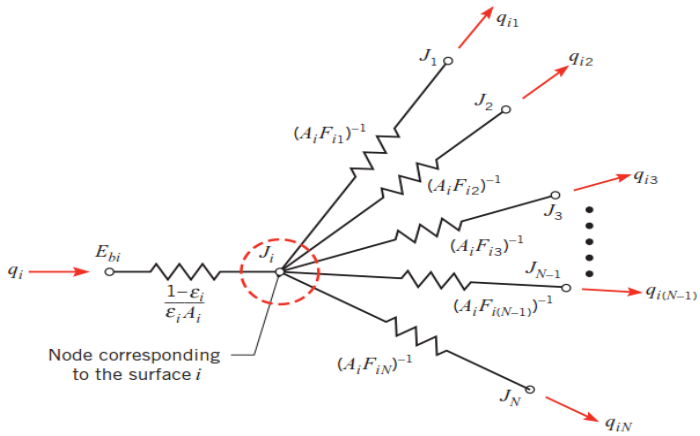

Figure 2.2: Network representation of radiative exchange between surface i and the remaining surfaces of an enclosure [17]

and not all the energy will reach the receiving surface. In this relatively simple scheme it's considered that the remaining surfaces don't radiate between themselves and this assumption makes possible the calculation of the initial heat flow by the following way:

$$q_i = \sum_{j=1}^{N} \frac{J_i - J_j}{\frac{1}{A_i F_{ij}}} = \sum_{j=1}^{N} A_i F_{ij} \sigma (T_i^4 - T_j^4) \tag{2.16}$$

Analysing it as a circuit problem (analogy problem), the current reaching a node will be equal to the sum of all the currents that leave the node.

Calculating the view factors by computational methods can be done through the Nusselt's hemicube method [18] which may be used to computationally estimate the view factors. If two surface patches are distant from each other, relative to their size, the inner integral in Eq. 2.14 varies little across the surface of A_i. In such a case, the form factor can be computed as that from a point to a finite area. If we project an element radially onto a hemisphere centered at that point and then project it orthogonally down onto the base, the fraction of the base area covered by this projection is equal to the form factor. This is the so-called Nusselt analog. This observation forms the basis of the hemicube algorithm, in which elements are projected onto a hemicube centered at the given point, as illustrated in Fig. 2.3.

In Fig. 2.3, the hemicube schematic is presented, in which the component ϕ represents the θ referred in the previous equations expressed along this chapter and where it can observed that the hemicube

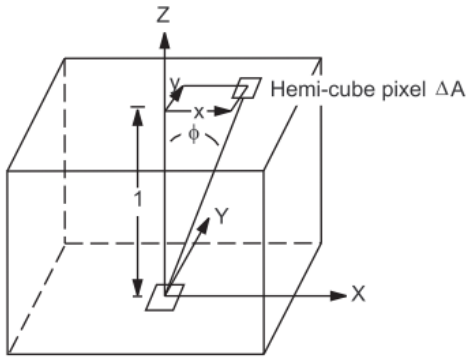

Figure 2.3: Schematic of the hemicube method present in [18]

sides are subdivided into N grid cells, named pixels, and can be expressed as follows:

$$F_{ji} = \sum_{j=1}^{N} \Delta F_n = \frac{cos(\theta_i)cos(\theta_j)}{\pi R_{ij}^2} \Delta A_j \tag{2.17}$$

where N is the number of pixels created and ΔF_n is the view factor between the reference surface and each of the target pixels.

2.2.0.3 Internal Heat Generation

In this study, internal heat generation is the process due to the collision of emitted neutrons with the atoms present in the body. These neutrons will pierce through the body, transmitting kinetic energy to each of the atoms hit by them, originating an internal source of energy/heat.

This heat source can be treated as a heat flux [19] and may be expressed as:

$$F_2 = \frac{1}{A} \int_A dA \int_{E_p} dE_p \int_{d\gamma} 4\pi\phi(r_s, E_p, \gamma) d\gamma \tag{2.18}$$

where A is the area of the body surface, E_p is the energy of each particle passing through the body and γ is the body's cross section.

Moreover, the heat generation present inside the structure is also considered and may be expressed as [19]:

$$F_6 = \frac{\rho_a}{V\rho_g} \int_V \int_t \int_{E_p} H(E_p)\phi(r, E_p, t) dE_p dt dV \tag{2.19}$$

where where t represents the discharge time, V the volume, ρ_a the atomic density, ρ_g the mass density, $\phi(r, E_p, t)$ the particle flux and $H(E_p)$ the heating response.

2.3 Finite Element Method

In order to solve both thermal and static problems, FEM is used to solve the differential equations inherent to these processes. When using this method, small sub-structure are created (known as finite elements) as the result of the discretization of the domain of either differential or integral equations.

These FE are connected (independently from their form) at points that are known as nodes (see Fig. 2.4), which must obey certain compatibility conditions on the primary variables, such as equal displacement or temperature continuity, depending on the problem addressed.

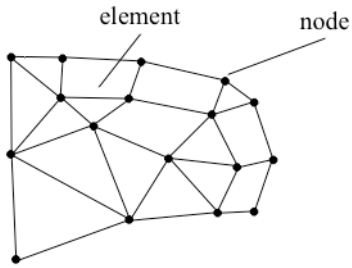

Figure 2.4: Discretized domain with finite elements and nodes [20]

This process can be mathematically formulated in two different ways. One is through the Galerkin's method [21], where FE's are found by establishing the variational formula and using local boundary conditions. Other method can result from an element-wise *Rayleigh-Ritz* treatment [22]. Since the FEM software used in this work (*ANSYS*) uses the first approach, this will be the mathematical formulation for the problem here present.

In order to apply the FEM, one must follow a certain number of steps [23]. This path is initiated with the creation of FE's, where the domain is discretized and originating a mesh (set of elements and nodes). Then it is necessary to calculate the weak form of the differential equations through the residual theorem or variational methods followed by Galerkin's method [24] in order to determine the elementary equations of the FE's. After this, the global system of equations is formed which will describe the analysis domain and the boundary conditions are set, whose number will depend the degree of the differential equation related to the event in question. To finalize, the system of equations is solved and the information wanted is retrieved.

The Finite Element Analysis (FEA) at hand is governed by the heat transfer equation that may be expressed as [25]:

$$-(\frac{\partial q_x}{\partial x}+\frac{\partial q_y}{\partial y}+\frac{\partial q_z}{\partial z})+Q=\rho c\frac{\partial T}{\partial t} \tag{2.20}$$

where q_x,q_y and q_z represent the heat flow components, Q is the internal heat generation, ρ is the material density, c is the material heat capacity, T is the temperature and t is the time:

$$q_x=-k\frac{\partial T}{\partial x}q_y=-k\frac{\partial T}{\partial y}q_z=-k\frac{\partial T}{\partial z} \tag{2.21}$$

Appying the Fourier's law to Eq. 2.20, the result is the following:

$$\frac{\partial}{\partial x}(k\frac{\partial T}{\partial x})+\frac{\partial}{\partial y}(k\frac{\partial T}{\partial y})+\frac{\partial}{\partial z}(k\frac{\partial T}{\partial z})+Q=\rho c\frac{\partial T}{\partial t} \tag{2.22}$$

As mentioned in [26], it is assumed that boundary conditions can be of the following types:

- Specified temperature

- Specified heat flow
- Convection boundary conditions
- Radiation

In this work, the only boundary conditions that are used are Specified temperature and Radiation, leading to the respective equations:

$$T_s = T(x, y, z, t) \text{ on } S_1 \tag{2.23}$$

and

$$q_x n_x + q_y n_y + q_z n_z = \sigma \varepsilon T_s^4 - \alpha q_r \text{ on } S_4 \tag{2.24}$$

where n_x, n_y and n_z are the components of the normal unit vector to the surface and $q_r^{"}$ is the incoming heat flow per unit area.

With a domain V divided into finite elements connected at nodes, shape functions N_i are used for interpolation of temperature inside a finite element:

$$T = [N]\{T\} \tag{2.25}$$

where $[N]$ is a matrix of shape functions:

$$[N] = [N_1 \; N_2 \; \cdots] \tag{2.26}$$

and $\{T\}$ is a vector of temperatures at nodes:

$$\{T\} = [T_1 \; T_2 \; \cdots] \tag{2.27}$$

Differentiation of the temperature interpolation equation gives the following interpolation relation for temperature gradients:

$$\begin{Bmatrix} \partial T/\partial x \\ \partial T/\partial y \\ \partial T/\partial z \end{Bmatrix} = \begin{bmatrix} \partial N_1/\partial x & \partial N_2/\partial x & \cdots \\ \partial N_1/\partial y & \partial N_2/\partial y & \cdots \\ \partial N_1/\partial z & \partial N_2/\partial z & \cdots \end{bmatrix} \{T\} = [B]\{T\} \tag{2.28}$$

Using the Galerkin method [24] in Eq. 2.20, one obtains the following result:

$$\int_v \Big(\frac{\partial q_x}{\partial x} + \frac{\partial q_y}{\partial y} + \frac{\partial q_z}{\partial z} - Q + \rho c \frac{\partial T}{\partial t} \Big) N_i dV = 0 \tag{2.29}$$

which through the application of the Divergence Theorem transforms into the subsequent form:

$$\int_V \rho c \frac{\partial T}{\partial t} N_i dV - \int_V \Big[\frac{\partial N_i}{\partial x} \frac{\partial N_i}{\partial y} \frac{\partial N_i}{\partial z} \Big] \{q\} dV = \int_V Q N_i dV - \int_S \{q\}^T \{n\} N_i dS \tag{2.30}$$

with $\{n\}$ being the outer normal vector to the surface of the body and:

$$\{q\} = -k[K]\{T\} \tag{2.31}$$

Through the application of the thermal constraints present in this study, one obtains the following equation:

$$\int_V \rho c \frac{\partial T}{\partial t} N_i dV - \int_V \Big[\frac{\partial N_i}{\partial x}\frac{\partial N_i}{\partial y}\frac{\partial N_i}{\partial z}\Big]\{q\}dV = \int_V Q N_i dV - \int_{S_1} \{q\}^T\{n\}N_i dS - \int_{S_4} (\varepsilon\sigma T^4 - \alpha q_r^{"})N_i dS \tag{2.32}$$

which traduces in the following final equation [27]:

$$[\mathrm{C}]\{\dot{\mathrm{T}}\} + [\mathrm{K}_T]\{\mathrm{T}\} = \{\mathrm{R}_T\} \tag{2.33}$$

where $[\mathrm{C}]$ and $[\mathrm{K}_T]$ are the general global specific heat and conductivity matrices, and $\{\mathrm{R}_T\}$, $\{\mathrm{T}\}$ and $\{\dot{\mathrm{T}}\}$ are the general global thermal load, temperature, and the first derivative of the temperature vectors, respectively. Hence, $\{\mathrm{K}_T\}$ is composed as follows:

$$[\mathrm{K}_T] = [\mathrm{K}_k] + [\mathrm{H}_{conv}] + [\mathrm{H}_{rad}] \tag{2.34}$$

where $[\mathrm{K}_k]$, $[\mathrm{H}]$ and $[\mathrm{H}_{rad}]$ are the global conductivity, convection and radiation matrices. Besides this, $\{\mathrm{R}_T\}$ has the following form:

$$\{\mathrm{R}_T\} = \{\mathrm{R}_B\} + \{\mathrm{R}_{conv}\} + \{\mathrm{R}_{h_{rad}}\} + \{\mathrm{R}_Q\} \tag{2.35}$$

where $\{\mathrm{R}_B\}$,$\{\mathrm{R}_h\}$,$\{\mathrm{R}_{h_{rad}}\}$ and $\{\mathrm{R}_Q\}$ are the global heat flux, convection, radiation and heat generation vectors, respectively. The FEA is established as a nonlinear transient thermal analysis (as radiation is considered and the properties of the materials are temperature dependent) that considers conduction and radiation effects (convection is not considered in this work as the medium is vacuum, which means that $[\mathrm{H}_{conv}] = \{\mathrm{R}_h\} = 0$ to estimate the temperature distribution along the antenna).

Regarding the elasticity field, a few other components must be taken into account. This way the following equation must be considered:

$$\prod = \int_V \frac{1}{2}\{\varepsilon^e\}^T\{\sigma\}dV - \int_V \{u\}^T\{p^V\}dV - \int S\{u\}^T\{p^S\}dS \tag{2.36}$$

where $\{p^V\}$ is the vector characterizing body forces and $\{p^S\}$ is the vector characterizing surface pressures, $\prod$ the total potential energy and $\{u\}$ is the vector for the displacements inside a FE. In order to transform Eq. 2.36 into a more known form, one must first know the following relations:

$$\{u\} = [N]\{q\} \tag{2.37}$$

and

$$\{\varepsilon\} = [\mathrm{B}]\{q\} \tag{2.38}$$

Mixing Eqs. 2.1, 2.36, 2.37 and 2.38, one is able to achieve the following equation:

$$\prod = \int_V \frac{1}{2}([\mathrm{B}]\{q\} - \{\varepsilon^t\})^T[\mathrm{E}]([\mathrm{B}]\{q\} - \{\varepsilon^t\})dV - \int_V ([\mathrm{N}]\{q\})^T\{p^V\}dV - \int_S ([\mathrm{N}]\{q\})^T\{p^S\}dS \quad (2.39)$$

From here, knowing that the minimum potential energy establishes that the minimum total potential energy takes the subsequent value:

$$\left\{\frac{\partial \prod}{\partial q}\right\} = 0 \quad (2.40)$$

then, Eq. 2.39 takes the following form:

$$\int_V [\mathrm{B}]^T[\mathrm{E}][\mathrm{B}]\{q\}dV - \int_V [\mathrm{B}]^T[\mathrm{E}]\{\varepsilon^t\}dV - \int_V [N]^T\{p^V\}dV - \int_S [N]^T\{p^S\}dS = 0 \quad (2.41)$$

or, in the matricial form:

$$[\mathrm{K}]_e\{q\}_e = \{p\}_e + \{h\}_e = \{f\}_e \quad (2.42)$$

where $[\mathrm{K}]_e$ is the element stiffness matrix, $\{h\}_e$ is the thermal vector and $\{p\}_e$ is the forces vector, where each take the following forms:

$$[\mathrm{K}]_e = \int_V [\mathrm{B}]^T[\mathrm{E}][\mathrm{B}]dV \quad (2.43)$$

$$\{h\}_e = \int_V [\mathrm{B}]^T[\mathrm{E}]\{\varepsilon^t\}dV \quad (2.44)$$

$$\{p\}_e = \int_V [N]^T\{p^V\}dV + \int_S [N]^T\{p^S\}dS \quad (2.45)$$

Afterwards, a static structural FEA, which may be expressed by Eq. 2.46, is conducted to evaluate the respective thermal displacements on the antenna:

$$[\mathrm{K}]\{U\} = \{F\} \quad (2.46)$$

where $[\mathrm{K}]$ is the global stiffness matrix, $\{F\}$ is the global force vector and $\{U\}$ is the global displacement vector that accounts for the thermal strain vector [27].

2.3.1 Finite Elements in ANSYS

The developed FE models feature SOLID186, which is a 3D 20-node structural-thermal FEs (see Fig. 2.4) has four degree-of-freedom at each node (displacements in the three directions and temperature). Furthermore, a 3D layered shell element SHELL131 is used (see Fig. 2.5) having four nodes with up to 32 temperature degrees of freedom at each node. For radiation, SURF252 is used in which surface loads can be overlaid onto a face of any 3D thermal solid or shell element that supports temperature degree of freedom. This SURF element is applicable to 3-D thermal analyses (see Fig. 2.6) and is

employed by overlaid on a face of the 3D thermal FEs.

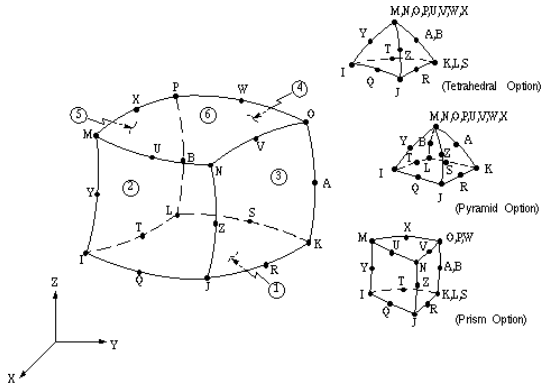

Figure 2.5: 3D structural-thermal FE SOLID186.

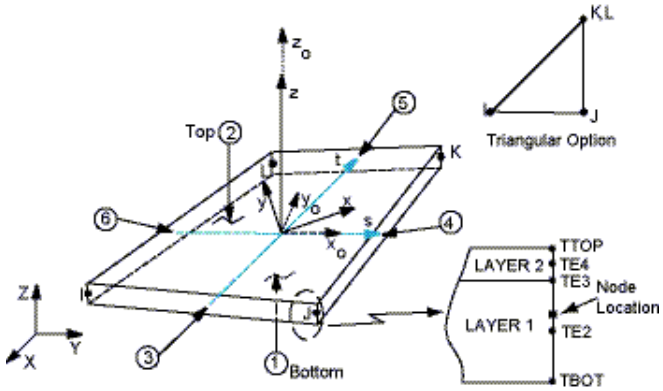

Figure 2.6: 3D layered shell element SHELL131.

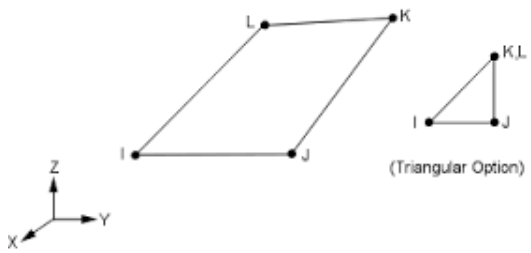

Figure 2.7: 3D thermal solid or shell FE SURF252.

2.4 Optimization Algorithms

In this section, a brief introduction to the algorithms used in the optimization processes is done. The general equation that precedes any of the performed optimization processes can be expressed in the following way [28], where its hybrid behaviour allows it to represent both single and multiple objective

objective functions:

$$\begin{aligned} &\underset{\mathbf{x}}{min}\, \mathrm{f}(\mathbf{x}) = (f_1(\mathbf{x}), f_2(\mathbf{x}), ..., f_k(\mathbf{x})) \\ &s.t. \\ &h_i(\mathbf{x}) = 0, i = 1 \text{ to } z, \\ &g_j(\mathbf{x}) \leq 0, j = 1 \text{ to } m. \end{aligned} \tag{2.47}$$

where k is the number of objective functions, z and m are the number of equality and inequality constraints, respectively, f(**x**) is the k-dimensional vector of the objective functions.

2.5 Topology Optimization

The designation of topological optimization is usually applied to a specific area of structural optimization dealing with the distribution of material densities along a permissible domain.

Although there are several TO methods, the method used in this work is the so-called "power-law approach", Solid Isotropic Material with Penalization (SIMP) [5]. In this approach, the material properties are assumed constant within each element used to discretize the design domain in which the stiffness is proportional to density in the power p (>1). As higher is p, the most the optimization results are "black-and-white", i.e., either additional material is present in that element or it is not and its formulation comes as follows:

$$E_i = \rho_i^p E_0,\ \rho \in]0, 1] \tag{2.48}$$

where E_0 is is the elastic property of the solid material, ρ is the element relative density (0< $\rho_{min} \leq \rho \leq$1) and E_i is element Young's modulus. Although this is the classic definition of the SIMP method, a more modern approach was developed [29], solving some of its issues:

$$E_i = E_{min} + \rho_i^p (E_0 - E_{min}),\ \rho \in]0, 1] \tag{2.49}$$

where E_{min} is the elastic modulus of the void material, which is always ρ >0 to avoid computational issues.

The compliance structural TO is the optimal density distribution that minimizes flexibility, i.e. to maximize the stiffness, which can be achieved by minimizing the compliance or by minimizing the elastic strain energy $\mathbf{C}$ [30], as follows:

$$\begin{aligned} &find\, \boldsymbol{\rho} = (\rho_1, \rho_2, ..., \rho_i, ..., \rho_{n_d}),\ 0 < \rho_i \leq 1,\ i = 1, 2, ..., n_d \\ &\underset{\boldsymbol{\rho}}{min}\, \mathbf{C} = \frac{1}{2}(\mathbf{f} + \mathbf{G})^T \mathbf{u} \\ &s.t. \\ &\mathbf{f} + \mathbf{G} = \mathbf{K}\mathbf{u} \\ &V \leq V_{(U)} \end{aligned} \tag{2.50}$$

where ρ_i is the pseudo-density variables, n_d is the number of densities variables, $\mathbf{f}$ is the external load

vector, $\mathbf{G}$ the self-weight load vector, $\mathbf{u}$ is the nodal displacement vector and $\mathbf{K}$ is the structural global stiffness matrix. Furthermore, V is the total volume of the material used for the structure with and $V_{(U)}$ is the prescribed upper limit.

2.5.1 ASO Method Algorithms

Adaptive Single Objective (ASO) is a single objective optimization process that is able to find a global optimum point by an evolving system that involves several subprocesses such as Optimal Space-Filling Design (OSF), Kriging and Mixed-Integer Sequential Quadratic Programming (MISQP), that ate going to be discribed next.

In the first optimization process the ASO tool is chosen to perform a parametric optimization aiming to decrease the ocurring maximum temperature T_{max} in the antenna. This process is expressed by a sort of parametric study, where the algorithm can assess each design found and decide in which direction should it continue. In other words, the program is capable of finding the best possible answers to the problem, given the limits inserted by the user.

As this is an algorithm based on decisions made by the program, it follows a workflow that allows it to do so, as illustrated in Fig. 2.8:

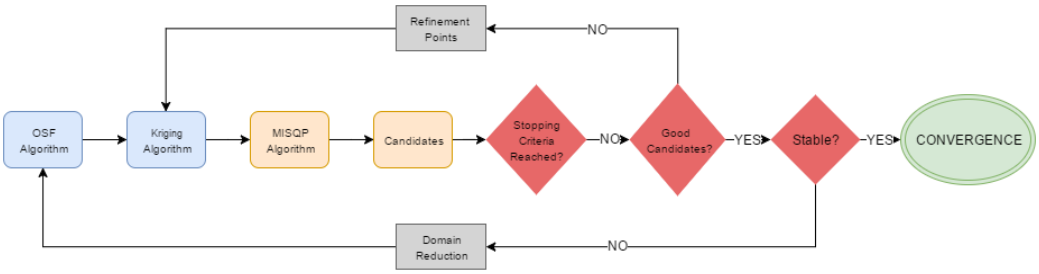

Figure 2.8: ASO workflow.

In Fig. 2.8 are presented the main steps of the procedure adopted by ASO and how each of this steps can correlate with another until the global optimum point is found (convergence). In a simplified way, the chain of events starts with the Optimal Space-Filling Design (OSF) algorithm, which will be responsible for generating the initial population with a uniform design point distribution along the selected design space. Following this step, the Kriging [31, 32] algorithm will be responsible for creating a response surface where the optimization will act. Having these pre-processing steps concluded, the MISQP [33, 34] optimization algorithm is applied and it will choose the best existing candidates. After this, these candidates will be subjected to a series of control steps, where these will determine the convergence or not of the values. The first control step will verify if any stopping criteria was reached (which would make the algorithm to stop if it did). The second control step will attest the quality of the candidates based on the *Kriging Error Predictor* [25]. A positive answer here leads to the next step in the chain but if a negative answer is reached, the *MISQP* algorithm will be restarted containing the rejected candidates.

The last control step checks the stability of the candidates, i.e. if all of the MISQP processes run on the response surface converge to the same verified candidate point. In case the convergence during MISQP is not achieved, a domain reduction will be performed through *OSF* around the candidates and

the process will be restarted. In case stability is verified, convergence is achieved and the final results are found.

There are two cyclic control steps, where in case of a negative answer the chain will be recommenced from the place it suits best.

2.5.1.1 OSF

Optimal Space-Filling Design is the algorithm responsible for generating the initial population of design points, guaranteeing that these points are equally dispersed throughout the design space established. OSF is a method derived from another sampling method called Latin Hypercube Sampling (LHS), working as an extended version of it.

In a generall way, LHS is a sampling method that generates random initial points along the design space but doesn't allow two equivallent points to be created [35].

2.5.1.2 Kriging model

In a general way, Kriging is a regression interpolation algorithm that provides an improved quality of the results obtained. Through its capability to estimate the internal error it can generate refinement points that will improve the Response Surface created, by filling the spaces where coherent data is in deficit, originating a Response Surface.

Kriging general model can be expressed in the following way, as seen in [31, 32]:

$$y(x) = \sum_{i=1}^{k} \beta_i f_i(X) + Z(x) \tag{2.51}$$

where k is the number of specified functions $f_i(x)$, β_i are the the unknown coefficients and $Z(x)$ is the realization of a normally distributed Gaussian random process with mean zero, variance σ^2, and nonzero covariance, which creates "localized" deviations so that the Kriging model interpolates the N sample data points. Further, the covariance is given by:

$$Cov[Z(x^i), Z(x^j)] = \sigma^2 R([r(x^i, x^j)]) \tag{2.52}$$

where R represents the correlation matrix and $r(x^i, x^j)$ is the spatial correlation of the function between any two of the N sample points and that can be expressed as:

$$r(x^i, x^j) = exp(-\sum_{k=1}^{d} \theta_k |x_k^i - x_k^j|^2) \tag{2.53}$$

with θ_k being the unknown parameters used to fit the model, d the number of design variables and x_k^i, x_k^j are the kth components of the sample points x^i and x^j.

2.5.1.3 MISQP

Mixed-Integer Sequential Quadratic Programming (MISQP) is an implementation of a Sequential Quadratic Programming (SQP) method. This is a method that solves Mixed-Integer Non-Linear Programming (MINLP) that is expressed in the following form as seen in [33, 34]:

$$\begin{aligned} & min\, f(x,y) \\ & s.t. \\ & g_j(x,y) = 0, j = 1,...,m_e \\ & g_j(x,y) \geq 0, j = m_e + 1,...,m \end{aligned} \tag{2.54}$$

where x and y are the continuous and integer variables vectors, respectively.

MISQP can be applied to convex and non-convex MINLP's [36], but assumes that the values of the nonlinear functions $f(x,y)$ and $g(x,y)$ do not change drastically as a function of y. MISQP implements a modified sequential quadratic programming (SQP) method, where functions are only evaluated at points (x,y) with y integer. It targets applications where the evaluation of $f(x,y)$ or $g(x,y)$ may be expensive.

2.5.2 AMO Method Algorithms

Adaptive Multiple Objective (AMO) is a multiple optimization process that, as in the ASO case, is able to find a global optimum point. This is achieved using several subprocesses that will create a multi-direction chain using Kriging or Multi Objective Genetic Algorithm (MOGA) algorithms.

In an analog way to ASO, it is strongly supported by preceding parametric results, which will reveal what will be the best compromise between goals, i.e., what will be the best values range to perform optimization once both objectives have slightly different action zones. Also as in ASO process, AMO procedure will be decided by algorithms and consequent evaluations in order to progress in the workflow presented in Fig. 2.9:

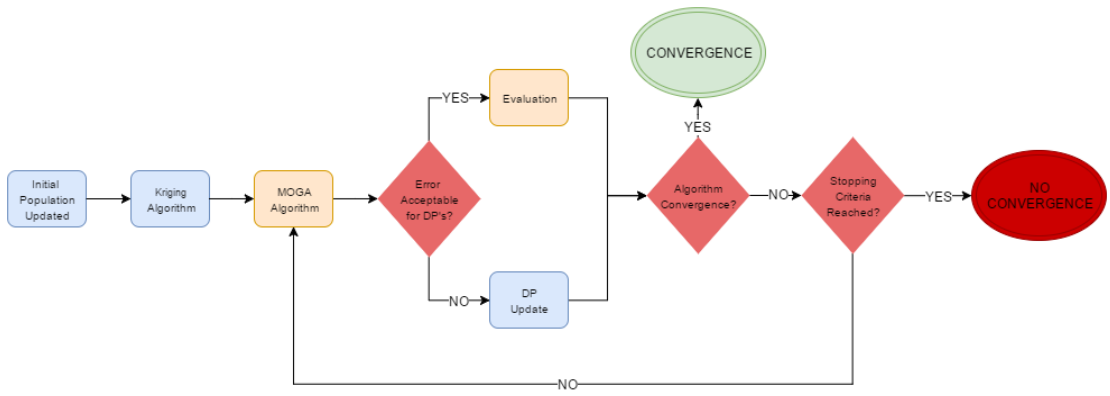

Figure 2.9: AMO workflow

The workflow expressed in Fig.2.9 presents, in an analogous way to the previous workflow presented in Fig. 2.8, the main steps followed during the AMO analysis and how they relate to each other. The initial population is generated through OSF that is the staring point for the response surface creation

by the Kriging algorithm. As in the previous case, this response surface is used by the optimization algorithm, in this case the multiobjective MOGA, to generate the best candidates. From here, a series of control control steps will decide the course to be followed, where the first control stop verifies if the error for each design point is acceptable. This is achieved through the *Kriging Error Predictor* where a positive answer will lead to the inclusion of the correspondent points in the next population to be run through MOGA until the number of samples defined is reached. In case the answer is negative, the points will be transferred to the *Kriging* step, in order to improve the response surface.

After this step, the next control point will verify if there is convergence (maximum allowable Pareto percentage has been reached). If the answer is positive, the final results have been found and the global algorithms stops. Otherwise, the chain will move forward to the next control step, where it will be checked if any stopping criteria has been reached. Here, if the answer is positive, the algorithm will stop and no answer will be found for the problem, once convergence was not reached. In case the answer is negative, *MOGA* will be run again. Although the main goal is to reach convergence, this might not be possible due to user input data limitations or process incompatibilities and in a ultimate case convergence may not be reached.

2.5.2.1 Kriging

This step will occur as in the ASO workflow, acting both on initial population generated as in all new populations created with MOGA.

2.5.2.2 MOGA

Multi Objective Genetic Algorithm (MOGA) is an optimization tool oriented for multiple objective problems based on the principle of natural genetics and evolution. Starting with an initial random population, the genetic algorithm exploits the information contained in the present population and creates a new population through via two main processes: Crossover and Mutation [37].

Crossover process

The Crossover process can be explained through an analogy of biology genetic recombination, where two chromosomes pair up with each other and exchange different segments of their genetic material to form new chromosomes. Here, the best features from each chromosome are chosen to form a new chromosome that can be better than its predecessors. This mechanism divides itself in two options, depending on the parameters being continuous or discrete.

For the continuous parameters case, two chromosome vectors are linearly combined, forming two descendant chromosomes as follows:

$$\begin{aligned} DescendantChromosome1 &= a \times chromosome1 + (1-a) \times chromosome2 \\ DescendantChromosome2 &= (1-a) \times chromosome1 + a \times chromosome2 \end{aligned} \tag{2.55}$$

where a is a random number that varies between 0 and 1.

Regarding the discrete parameter case, each will be represented by a binary chain that corresponds to the number of values:

$$N_v = 2(n-1) \tag{2.56}$$

with n being the number of bits in the chain. These chains can be viewed as genes that connecting to each other create a chromosome, that performs crossover with another. This mechanism can be executed in three ways, depending on the place in the binary chain where the separation in made. If it's *One-Point*, a certain point in the chain will be the break-up point, i.e., the point from where the posterior piece of chain will leave to be combined with another chain and where the piece split from that chain will combine with the first. A similar process occurs in *Two-Point*, where the remaining piece of chain will be located between points as shown in Fig. 2.10:

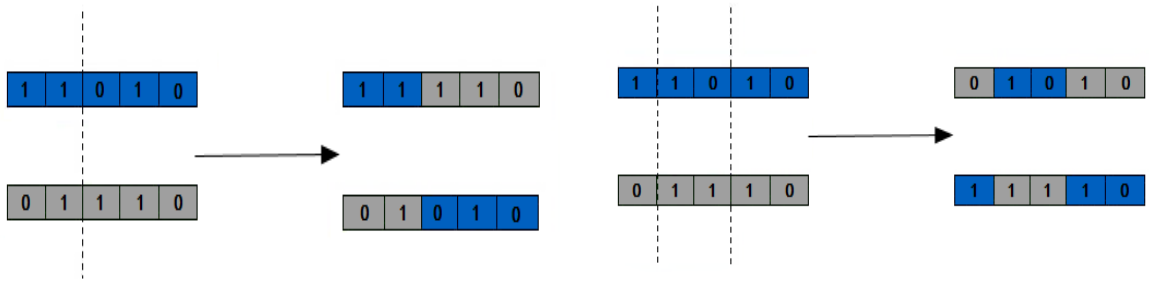

(a) One-Point Crossover (b) Two-Point Crossover

Figure 2.10: Crossover schemes

The last mode of performing crossover with discrete parameters is called *Uniform* and in it there is a random swap of genes and not segments of chain which can increase the diversity of the resulting chromosome.

Mutation process

The Mutation process is responsible for inserting new genetic information into the population where the resulting chromosome is altered in a random way. This procedure is crucial to the evolution of the whole operation, once it allows the population to move forward when finding a local optimum but, as in the previous case, it has different approaches depending on the nature of the parameters.

When continuous parameters are present, a polynomial mutation operator is employed to achieve mutation as follows:

$$R_c = I_c + (UpperBound - LowerBound) \times \delta \tag{2.57}$$

where R_c is the mutation resulting chromosome, I_c and δ is a small variation calculated from a polynomial distribution.

For the discrete parameters case, a mutation operator simply inverts the value of the chosen gene (since in this situation we're treating binary data, 0 turns to 1 and vice versa).

2.5.2.3 Weighted Objective Function

When having two or more objectives colliding in a single final objective, it's necessary to define the weight that each objective will have in the final result. Concerning this, a method for defining the final objective function is developed in the following way [38]:

$$\phi = \sum_{i=1}^{n} w_i N_i + \sum_{j=1}^{m} w_j M_j \tag{2.58}$$

where w_i and w_j are the weights of input and output parameters, respectively and can possess the values of 1, 0.666 or 0.333 depending on their "importance" being defined as "Higher", "Default" or "Lower", respectively. On the other hand, N_i and M_j are the normalized objectives for input and output parameters, respectively. These last features can be expressed as:

$$N_i = (\frac{|x_t - x|}{x_u - x_l})_i \tag{2.59}$$

and

$$M_j = (\frac{|y_t - y|}{y_{max} - y_{min}})_j \tag{2.60}$$

where x and y correspond to the current value for input parameter i and output parameter j, respectively, x_t and y_t correspond to the target value, x_u and x_l match the lower and upper values, respectively, for input parameter i and finally y_{max} and y_{min} represent the lower and upper bounds, respectively, for output parameter j.

Regarding the input parameters, the x_t component can be expressed as follows:

$$x_t = \begin{cases} x, & \text{if Objective is defined as "No Objective"} \\ x_l, & \text{if Objective is defined as "Minimize"} \\ x_u, & \text{if Objective is defined as "Maximize"} \\ \frac{x_u + x_l}{2}, & \text{if Objective is defined as "Seek Target"} \end{cases} \tag{2.61}$$

Concerning the objectives definition, the output parameter component y_t, it can defined as:

$$y_t = \begin{cases} y, & \text{if Objective is defined as "No Objective"} \\ y_{min}, & \text{if Objective is defined as "Minimize"} \\ y_{max}, & \text{if Objective is defined as "Maximize"} \\ y^*, & \text{if Objective is defined as "Seek Target"} \end{cases} \tag{2.62}$$

If constraints type are defined, the same output parameter component y_t can have the following

expressions:

$$y_t = \begin{cases} y, & \text{if Constraint is defined as ”Values} \leq \text{Upper Bound” and ”Upper Bound” as } y \leq y_t^* \\ y_t^*, & \text{if Constraint is defined as ”Values} \leq \text{Upper Bound” and ”Upper Bound” as } y \geq y_t^* \\ y_t^*, & \text{if Constraint is defined as ”Values} \geq \text{Lower Bound” and ”Lower Bound” as } y \leq y_t^* \\ y, & \text{if Constraint is defined as ”Values} \geq \text{Upper Bound” and ”Upper Bound” as } y \leq y_t^* \\ y_{t1}, & \text{if Constraint is defined as ”Lower Bound”} \leq \text{”Values} \leq \text{Upper Bound” and } y \leq y_{t1} \\ y_{t2}, & \text{if Constraint is defined as ”Lower Bound”} \leq \text{”Values} \leq \text{Upper Bound” and } y \leq y_{t2} \\ y, & \text{if Constraint is defined as ”Lower Bound”} \leq \text{”Values} \leq \text{Upper Bound” and } y_{t1} \leq y \leq y_{t2} \end{cases} \tag{2.63}$$

where y_t^*, y_{t1} and y_{t2} are the user-specified target, the constraint lower bound and the constraint upper bound, respectively.

Chapter 3

Methodology

In the present work, the main objective is to study the thermal and structural effects of plasma infliction in the PPR Antenna and optimize this structure in order to reduce the resulting maximum ocurring temperature and displacement, i.e. $\mathrm{T}_{\mathrm{max}}$ and $\mathrm{D}_{\mathrm{max}}$.

This chapter presents information regarding the methodologies that are going to be applied. It includes the description of the model construction, followed by an explanation of Steady State Thermal and Static Structural analysis as well as the Ansys environment and the optimization tools to be used on the model.

3.1 Model Presentation

The reflectometry system located in GAP4 of ITER, is composed by several components, including the antenna that is the focus of this study. In [16], in a way of trying to simulate these components, as well as all the environment, a simplified CAD model was created from the original model illustrated in Fig. 3.1.

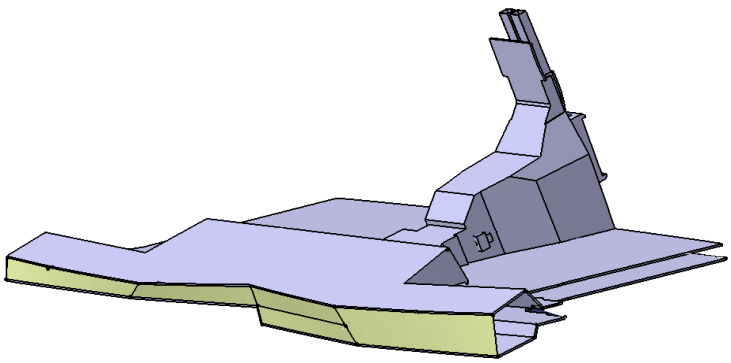

Figure 3.1: Original Enclosure Model [16].

Given the extremely high amount of computational time required on a single study with this model, a reduction of the model to one that would keep the main features to be studied and still present coherent results was made in this work and is also described in [39].

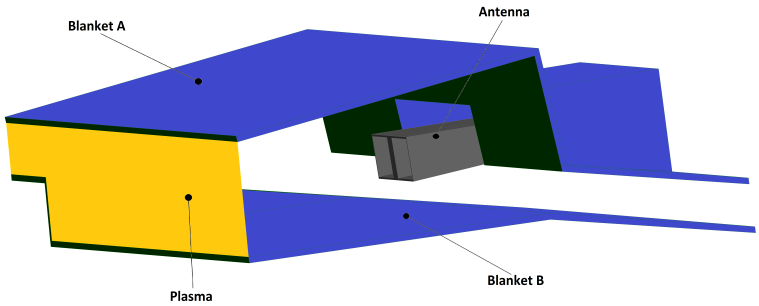

Figure 3.2: Simplified Enclosure Model.

In Fig. 3.2 the model used for both thermal and static studies is presented, where four components are visible. The first, colored in yellow is the plasma radiative surface, which as its name says, is responsible for the emission of the plasma. The second and third, colored in blue, are the blankets that consist in the components that represent the bodies surrounding the antenna in GAP4. Last but not least, colored in gray, the antenna located between blankets and facing the plasma surface.

The model presented reveals itself as a much simpler assembly, where the goal of this simplification resides in keeping the previous conditions for the antenna while reducing the computational process time, as many of these analysis are performed during the parametric studies. By this way, both blankets were cut in a way that both could still cover all the antenna, leaving still a small margin behind it as a security measure. Thus, all the components behind the antenna were removed, relieving the machine processing once only the remaining bodies will be handled.

The CAD system used model of the current antenna project, available in ITER's ENOVIA, is illustrated in Fig. 3.3.

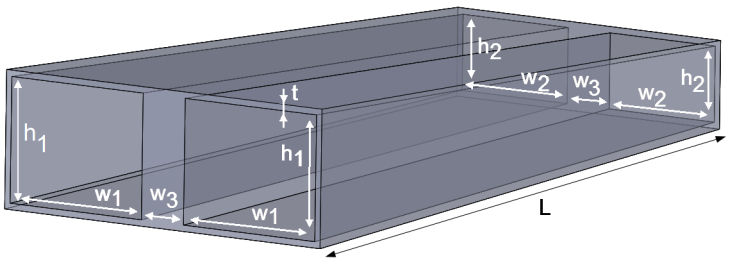

Figure 3.3: CAD model of ITER PPR antenna [w_i – width; h_i - height, t - thickness (uniform) and L - length].

In Fig.3.3, the dimensions of the antenna are also illustrated in their correct location, where each has the following designation: w-width, h-height, t-thickness (uniform) and L-length. All these dimensions are presented in Table 3.1, where their values are indicated:

Table 3.1: Dimensions of the ITER PPR antenna.

w_1 (mm)	w_2 (mm)	w_3 (mm)	h_1 (mm)	h_2 (mm)	t (mm)	L (mm)
25	20	8	20	12	1	115.4

Based on this model (Fig. 3.3), a parametrized FE model is developed to account for optimum

design as illustrated in Fig. 3.4. This new FE model portrays a coverage in the original antenna, where it contains two parameters, which consist in the length of antenna coverage L_c and respective thickness t_c that may vary within specific boundary values.

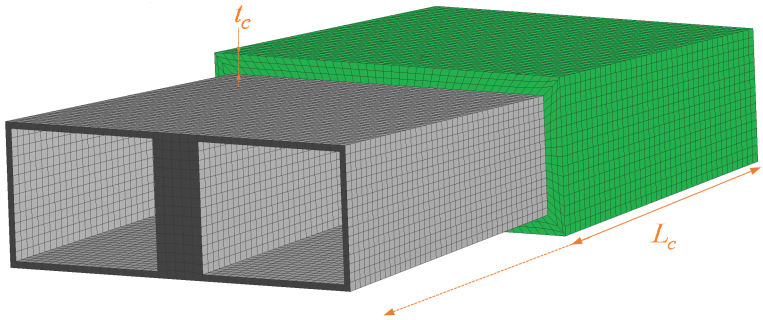

Figure 3.4: Parameterized CAD model of the antenna and its coverage: (w – width; h - height, t - thickness (uniform) and L - length).

The FE model illustrated in Fig. 3.4 and the remaining components of the general CAD model feature tri-dimensional 20-node structural-thermal FE's with four degree-of-freedom at each node (displacements in the three directions and temperature). For radiation, 3D radiosity surface FEs are employed, overlaid on a face of the 3D thermal FEs, as mentioned in section 2.3.

3.2 Parametric Design

In a primary approach, given the complexity of the antenna model, a simple structure was created so that simple studies can be applied to it. These studies will suit as a starting point on understanding how will the model behave while facing similar circumstances.

3.2.1 First Parametric Approach

When aiming to start a parametric study, first one has to define which parameters are meant to be analysed. In this particular case, the desired element is the antenna's thickness, but, as the interior dimensions must not be changed, only the exterior ones will be parametrized. From here, one has to decide how this exterior thickness will vary, in other words, we have to decide if it is better to change the thickness uniformly or if it is better to change each measure (bottom, top and lateral) separate from the others. Once it would be more effective to see which parts require more or less attention, it is best to follow the second path. This way, one obtains a sample of how the structure would be optimized when subjected to a certain situation.

Taking this in consideration, it is now possible to start drawing the part by the most appropriate method in order to prepare the structure to be optimized and to be easily altered when or if necessary. To do this, the program Solidworks [40] is used as the CAD creating software, in which one of the following procedures is to be followed:

- When aiming to a uniform thickness, only the interior design is used. A "Loft" feature is applied (Fig. 3.5(a)), originating a solid body between the two top rectangles. Following this, a "Shell"

command is put to use[Fig. 3.5(b)], in which it is direction is set as outwards in order to be able to choose this shell measure and define it as a parameter later;

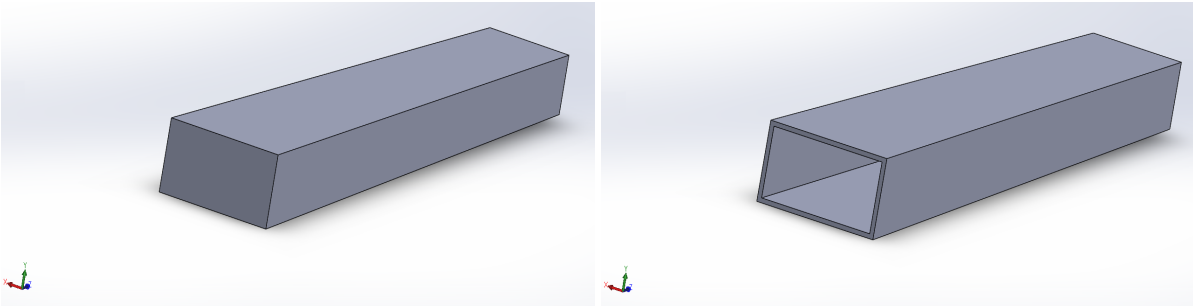

(a) Sketch loft creating solid.

(b) Shell command creating shell body.

Figure 3.5: Primary approach model first construction steps on Solidworks.

- If aiming to a non-uniform thickness, two drawings will be made: the interior and the exterior drawings. From here, a loft feature will be created between the outer sketches (Fig. 3.6(a)), leading to the formation of a solid body. Followed by a "Lofted Cut" command involving the inner sketches (Fig. 3.6(b)), a thickness is created which can be controlled by both of the sketches' measures. Once it is not desired to move the interior dimensions of the antenna, only the exterior dimensions will be altered and allowing the structure to have a non-uniform thickness.

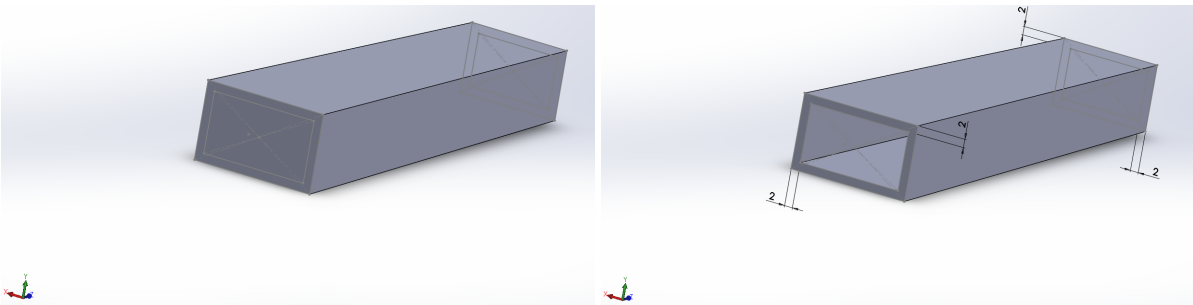

(a) Sketch loft creating solid.

(b) Loft cut command creating a non-uniform thickness on the body.

Figure 3.6: Primary approach model second construction steps on Solidworks.

As said before, it is required that the inner dimensions stay the same throughout all the processes, but, in order to have a stronger case when assessing the best resulting solid feature possible it is not wise to keep the thickness uniform, so, only the second method of construction will be considered. This can be achieved by fixing the inner dimensions and defining the distance between both dimensions as a parameter, allowing only the outer ones to be altered.

The last step of this chapter, is to enter the process of parameter definition. To do this, one starts by making our feature dimensions visible by selecting the "Display Annotations" option in the "Annotations" icon on the tree menu. Following this, we must access the "Evaluate" separator, open the "Design Study" menu and click on "Parameters". This will open a window (Fig. 3.7) with a list showing all the active parameters (which should be none at this time) and here one selects the dimensions wanted and

add them to the list.

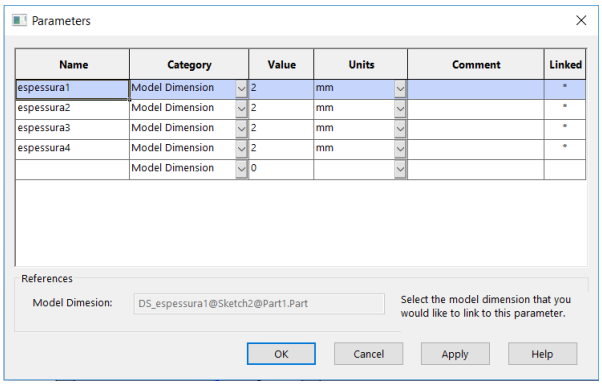

Figure 3.7: Design study parameters setting.

When all of the wished parameters were added, this window is closed and each of these dimensions must be accessed where their name must be changed in order to include one of two prefixes “DS” or “ANS” (Fig 3.8):

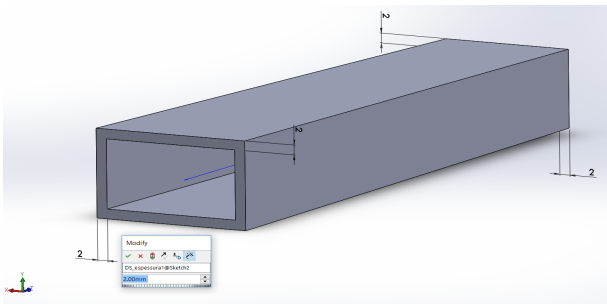

Figure 3.8: Design study parameters setting - prefix.

When all this is set, it is now possible to start the optimization process. By this way, and as mentioned before, the thickness will be parametrized in four different measures, regarding front and back thicknesses (horizontal and vertical) of the antenna. Then, the conditions which the part is subjected to are introduced in the form of two different type of analysis: Steady Thermal analysis (which is responsible for the thermal distribution along the body which is required to the Elastostatic analysis with thermal load) and a Static Structural analysis (which is responsible for the displacement and stress response taking into account the constraints and forces acting in the structure). This is achieved by importing the CAD model into the FEM software ANSYS Workbench.

This kind of optimization basically consists in defining one or more entities that one would like to see optimized and submit them to an algorithm responsible for deciding which will be the possible scenarios.

In the following parametric studies, the FE software Ansys Workbench [25] is used while different entities from the antenna are chosen to be evaluated. These entities will be defined as parameters and will be changed along each analysis performed, where the main diagnostic will be based on the maximum deformation and the maximum stress along all the structure. As such, looking at the antenna’s form, it was decided to parametrize the measures of its thickness, once it would be the best way to reveal which would be the best shapes in order to have the smaller deformation as well as the smallest stresses.

After performing the steps mentioned in the methodology chapter regarding the parametrization of our part, it becomes possible to start the optimization process. In an analogue way to the one used in the verification chapter, temperatures will be defined in the front and back of the antenna, simulating the action of the radiation that inflicts the body. This radiation causes a thermal difference of ΔT≅500°C, where a temperature of around 700°C is present on the front face of the body, and a temperature of around 200°C is present in the back face. This is responsible for a thermal load which causes a disturbance in the state of the rest of the antenna, as illustrated in Fig. 3.9.

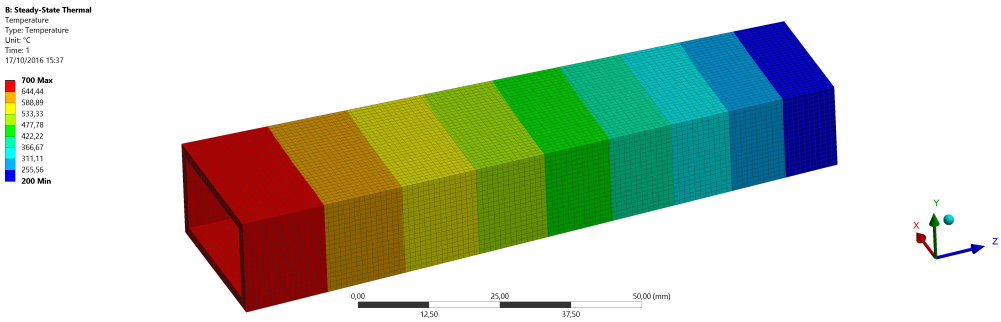

Figure 3.9: Temperature distribution with temperature constraints.

Following this step, the constraints must be set. As the study being performed does not have as a goal the examination of the stresses present, the type of constraint applied and its reliability towards the real condition of the model won't be preponderant. Therefore, the best procedure is to find the worst case scenario possible and this occurs when the body is fixed in its rear face.

As this is merely an exercise to understand how would a parametrized model with the present material properties [41] behave, the maximum stress σ_{max} is chosen as the optimization target. Knowing that this value will be located in the fixed face of the antenna (rear face), and given the material properties in [tabela] which fluctuate with the temperature, one sets as a objective the decrease of this σ_{max}. Then, the best procedure is to find the worst case scenario possible and this occurs when the body is fixed in its rear face.

After these steps, having all the loads and constraints necessary the time arrives to initiate the parametric optimization. In this study the Direct Optimization tool is used and it consists in a process already mentioned in section 2.5.2.2: the aleatory choice of user defined number of design points, where by looking at the parameters chosen as the main elements of decision, the best design points will be picked by the algorithm. With this method, an initial number of samples will have to be defined, as well as other components like the convergence tolerance or even the pretended number of best candidates generated.

At this point, the main decision parameter belonging to the antenna is the maximum stress present. The values of this parameter are minimized, becoming this the main goal of this study and the fifth parameter defined.

As the last parameter is already defined, the remaining four must be constrained in a range of values that will suit the purpose. Analysing the structure that can be seen in [16], one must define this range in a way that the antenna does not enter in conflict with other components. Thus, by looking at the full

antenna illustrated in Fig. 3.10, the range of values will go from 1 mm to 3,9 mm in order to comply with the requirements, once that only with 4 mm of thickness the structure will have both antennas united and 1 mm of thickness will be a reasonable number for the lower case and a gap between both is required.

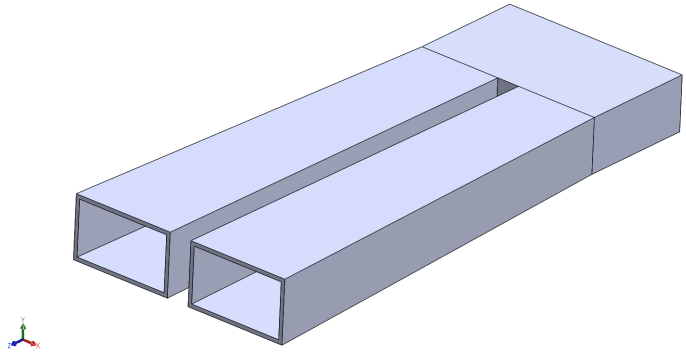

Figure 3.10: Complete antenna

Furthermore studies were made upon the results of the first analysis's, where the range imposed before restrained in compliance with the best resulting geometries, i.e. once the design points are aleatory, by restraining the range of values in different ways to different parameters and maintaining the number of geometries to be generated, it is possible that a more optimized structure will be found.

3.2.2 Final Parametric Design

Since the previous parametric design was only destined to infer how would a structure with a given material behave in similar conditions to the present project, a new and more complex design was made.

From the theoretical data explained in chapter 2, namely in the heat transfer section, it is possible to speculate that adding material to the antenna would improve the existing project objectives, namely the body temperature. Consequently, a new model was thought in a way that the user could perform similar tests in the structure being able to see the evolution of the results depending on the amount of material being added to the antenna. To achieve this, a homogeneous evolution would be more suitable, with this meaning that the augmented material would be placed equally in the four exterior surfaces of the model.

In the design phase of the final antenna, the process was very similar to the one used in the primary structure, where the solid formation depends mainly on lofts and lofted cuts. The main difference relies on the fact that now it is needed to parametrize both the ”height” of the material added and well as its length. So, the way of doing this goes through combining two bodies dependent on new plane sketches, i.e., three sketches present in three different planes and consequent lofts uniting them like demonstrated in Fig. 3.11: After the sketching step, the parameters have to be set, which will be made in an analog way to the previous CAD model, creating two parameters that are able to control the thickness and the length of the coverage added to the original antenna. The thickness parameter will be defined on the sketch in the rear of the antenna, measuring the space between the coverage sketch edge and the antenna's inner sketch edge, on the left side and both on top and bottom.

Regarding the length of the coverage, it will be controlled by a 3D line uniting the first sketch and

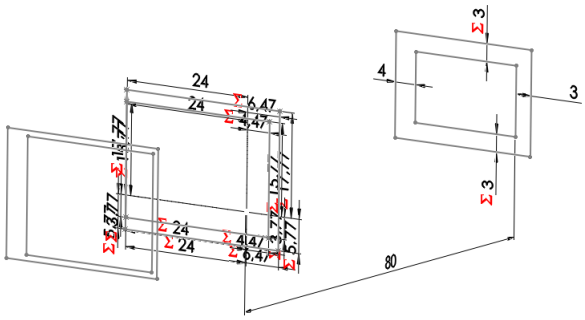

Figure 3.11: Sketches used in the model design and the main dimensions.

the plane where the next sketch will be placed. In this plane, the sketch will be divided in three parts: the inner antenna sketch, the original antenna external sketch and the coverage external sketch. This last subsketch (which is united with the first plane through a loft feature) is built based on points and lines connecting each other. Each point is governed by a simple equation of distance towards the model Coordinate Origin, which allows the coverage to keep up with the original structure's leaning on the sides, top and bottom in a homogeneous way.

When all these steps are concluded, the mirror feature is used with the Right Plane, originating the final result expressed in Fig. 3.12:

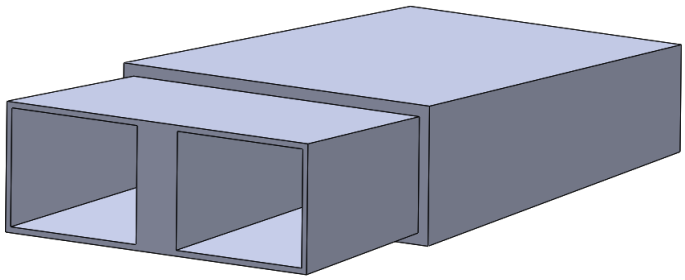

Figure 3.12: Final Parametric result of the antenna with coverage

Once again, after having the model created in Solidworks, it is imported to the FEM program ANSYS Workbench to perform all the analyses.

3.3 Topology Optimization Study

Regarding the second type of optimization, the initial steps of material definition and thermal loads will remain identical to the previous type of optimization. The process starts to change when we want to define static structural constraints. This step is now merged with the next step, which will consist in the topology optimization. Topology optimization is applied by means of the Beta tool present in Ansys Workbench and it is in this tool that the part constraints will be defined, right before the optimization algorithm.

The topology optimization tool, curiously named "Shape Optimization" (SO) runs an algorithm that

consists in the SIMP method described in the fundaments chapter. This algorithm analyses the structure, as well as its constraints and loads and it generates a geometry (in reality it is a distribution of material densities) that is be capable of fulfilling all the requirements given, in this case with a volume constraint, i.e. a percentage of the volume to eliminate will be defined.

In the last step of this method, one must pay attention to how the constraints will be imposed, for they will represent a major role in the optimization. Keeping in mind the idea that all the constraints must still be able to simulate the conditions in which the antenna is under, the constraints defined here will also influence the withdraw of material so an acute sense of engineering appraisement must also be present.

Beginning the definition of the body constraints, the previous settings will also be used here in order to simulate the real environment in which the antenna is immersed. If these were the only constraints, the tendency would be of retrieving material from the front part of the body, leaving only where it needs the most, i.e. the back of the antenna. It is here that the sense of engineering must enter, allowing to create more constraints so the resulting geometry can be of some use from the engineering point of view.

For the last step, the percentage of volume must be defined, which dictates the percentage of body to be removed. In this step, it was chosen as a primary study to use a 50% of volume removal, as this is not an extremely high value (which could eliminate the practical use and building of the resulting geometry) and it is not a low value, allowing the viewer to see the kind of effects that are to expect from this analysis. Once these resulting geometries cannot be used by the user after the analysis, a similar geometry must be sketch by the help of the same CAD software as before, looking only at the results obtained from before.

3.4 FEM Analysis

The tool used to perform FEM analysis in the present work is the ANSYS® Workbench, which has the intended requirements to perform both thermal and structural analysis.

As mentioned in subsection 3.2.2, the CAD model designed in Solidworks is imported to to ANSYS® Workbench in through the *Geometry* tool and consequently edited in *Design Modeler* tool, that is the subprogram that allows the user to pick the recognized parameters defined in Solidworks. In a similar way, the material properties of the model, which will be the same for all the components, are also imported to workbench through the *Engineering Data* tool.

Afterwards, the conditions are gathered to initialize the mesh FEM preceding steps. Firstly, the material is attributed to each model component and a virtual thickness of 1mm is attributed to the plasma surface in order to be recognized as physically present. Secondly, given the fact that for the parametric studies to be performed (continuously changing geometry), a relatively easy to generate mesh must be used, the option *Hex Dominant* in mesh tools was chosen for the model to be assessed. Furthermore, although the *Multizone* had a better mesh appearance, it would fail to generate a mesh in many cases, resulting in a failed study, a case that did not occur with the chosen option. Still in this tool, the option of *Element Midside Nodes* was set to *Kept* which, given the fact that 3D elements will be generated in the

antenna, will force the elements present to be of 20 nodes. Following this, a *Body Sizing* tool was also utilized to characterize the elements size for the model and consequently the element number present and served as a regulator for the convergence study for both thermal and static analysis.

3.4.1 Thermal Analysis

The first analysis to be performed in the model is one of thermal nature, in order to deduce the temperature distribution along the antenna, as well as the key factor $\mathrm{T}_{\mathrm{max}}$ magnitude and position in the structure. As there are no static force loads yet, no constraints are defined, only temperatures and emissivities are established here.

In Fig. 3.2 the model used for both thermal and structural studies is presented. An environment temperature of 150°C is assumed, while both A and B blankets have a temperature of 300°C defined in their interior surfaces, once these are the ones that interfere with the radiation process.

As the only source of energy present in the model is the plasma surface shown in yellow color in Fig. 3.2, this component radiates a power density of 500 kW/m^2 [42]. Given the fact that this energy is transferred by radiation, the equations expressed in section 2.2.0.2 is the basis to solve the problem, treating the surface as a black body. As in Eq. 2.7 the only parties are Stefan-Boltzmann constant σ and the temperature, which means that, considering σ always constant, only the temperature can influence the power density. Hence, a temperature of 1451°C was set on the yellow surface (Fig. 3.2 for this purpose.

Finally, only one more temperature was needed to be established. From [16] it is possible to see what is the approximated temperature in the rear side of the antenna, which, given the simplification of the model, doesn't have any components attached to it and so, a temperature must be established there to allow the study to keep its coherence. Consequently, a temperature of 300°C was set on the surface of the rear part of the component, completing the temperature setting process in the model.

The next step is to set the emissivities of each components, excluding the plasma surface, which has already been said to treated as a black body, i.e., its emissivity ε is equal to 1. Regarding the other components, the emissivity is equal to the one defined in [16] for the blankets and the antenna, with the exception of the rear face of the antenna, where, due to the fact that it is supposed to be attached to other pieces, is emitting radiation. It is further assumed that the surface emissivity is equal to the surface absortivity.

The last step is based on the implementation of nuclear heat load distribution, induced by the neutrons and gamma photons coming from the plasma and surrounding materials. These results are generated with the *Internal Heat Generation* option, where the values presented were estimated using the Monte Carlo simulation program MCNP6 [43] and ITER reference neutronics models provided by the ITER Organization, keeping in mind that the thermal loads due to ECRH/CTS stray radiation are not taken into account as they are considered negligible [44].

3.4.2 Elastostatic Analysis with an imposed distribution of temperatures

The second analysis implemented consists in a structural test that is meant to analyse the elastostatic response present in the model.

Coupling the *Steady Thermal* with a *ElastoStatic Structural* analysis as shown in Fig. 3.13, allows to connect the thermal analysis of the FEM with the elastostatic one. This means that both the mesh definitions and the material attributions (as well as the parameters already defined) will remain the same, allowing a continuous study to happen as a weak coupling form, i.e., the study will occur in one way where the posterior step doesn't need to return to the anterior one.

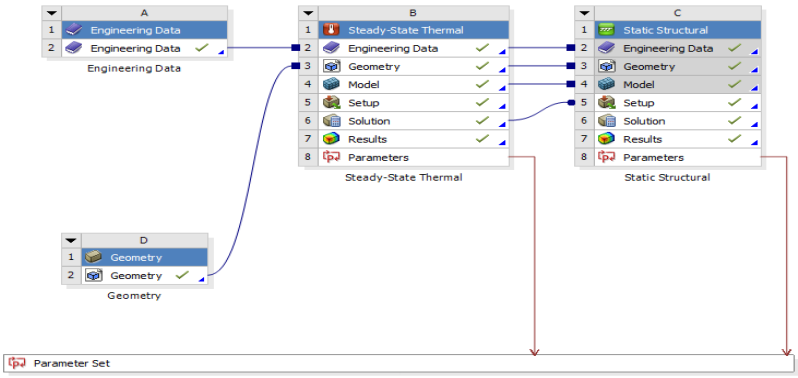

Figure 3.13: Ansys Workbench Workflow

This analysis has the purpose of finding the displacement distribution on the antenna and consequently the D_{max} magnitude and its location. In order to achieve this, the thermal load is imported from the *Steady Thermal* analysis and the action of the Earth Gravity in the structure, is activated so that it also also causes deformation.

As the full model is not oriented according to the design orientation of the antenna it is crucial to define a new coordinate system that follows this. Since Displacement D is the target of this study, it's of the greatest importance that the worst possible case scenario is represented and this happens when the acceleration acts in a parallel direction to both front and rear faces of the antenna in z direction of Fig. 3.14. The acceleration has the same direction as the *z* vector and this is set using the option available

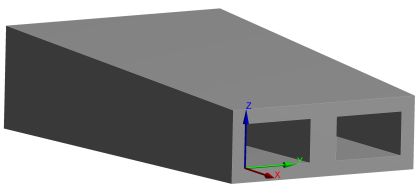

Figure 3.14: New coordinate system on the antenna.

Standard Earth Gravity. In this option, the acceleration magnitude is automatically set to 9,8066 m/s^2 and the user just has to choose the coordinate system and the negative direction for the acceleration too act.

The next step involves the setting of the model constraints. As the study being performed does not have as a goal the examination of the stresses present, the type of constraint applied and its reliability towards the real condition of the model won't be preponderant. In this case, as the goal is the maximum displacement present D_{max} only in the antenna, the best procedure is to find the worst case scenario possible and this occurs when the body is fixed in its rear face. Respecting the other components, their constraint is not of any importance as long as they keep their exact location, so a great number of faces were fixed in both blankets and the plasma surface was completely fixed, assuring that they were completely fixed.

3.5 Design Optimization

After both thermal and static studies are ready, it is possible to start the design optimization based on the parameters earlier defined. This optimization consists in the application of the two adaptive optimization tools provided by Workbench already introduced in section 2.4 and is strongly supported by the results obtained in the parametric studies for T and D.

3.5.1 ASO Optimization

Using Eq. 2.47, the ASO optimization general equation can be expressed as follows:

$$\begin{aligned} &\underset{\boldsymbol{L_c},\boldsymbol{t_c}}{min}\,\mathrm{T}(\boldsymbol{L_c},\boldsymbol{t_c}) \\ &s.t. \\ &L_{cmin} \leq L_c \leq L_{cmax} \\ &t_{cmin} \leq t_c \leq t_{cmax} \end{aligned} \tag{3.1}$$

where L_{cmin}, L_{cmax}, t_{cmin} and t_{cmax} are the minimum and maximum allowable length and thickness of the material coverage, respectively, T is the temperature. In Eq. 3.1, T is minimized while being subjected to L_c and t_c constraints.

3.5.2 AMO Optimization

AMO (Adaptive Multiple Objective) is a very similar optimization method to ASO where the main difference resides in its multiple objective nature. This aspect allows the program to evaluate the existing results based on the two objectives established and move in a direction that satisfies both, depending on how the user defines each weight, where the problem can be expressed as follows:

$$\begin{aligned} &\underset{\boldsymbol{L_c},\boldsymbol{t_c}}{min}(\mathrm{T}(\boldsymbol{L_c},\boldsymbol{t_c}),\mathrm{D}(\boldsymbol{L_c},\boldsymbol{t_c})) \\ &s.t. \\ &L_{cmin} \leq L_c \leq L_{cmax} \\ &t_{cmin} \leq t_c \leq t_{cmax} \end{aligned} \tag{3.2}$$

where L_{cmin}, L_{cmax}, t_{cmin} and t_{cmax} are the minimum and maximum length and thickness of the material coverage, respectively, T is the temperature, D is the displacement and **x** represents both parameters L_c and t_c. In this case, not only T but also D is minimized, while being subjected to L_c and t_c constraints.

Looking at Eq. 2.61, Eq.2.62 and Eq.2.63, the constraints defined in the software were set as $x_t = x_l$ and $y_t = y_{min}$ as the only objective present is to minimize (wether only T or both T and D). Given these expressions, the Eq.3.3 and Eq.3.4 become as follows:

$$N_i = \left(\frac{|x_l - x|}{x_u - x_l} \right)_i \tag{3.3}$$

and

$$M_j = \left(\frac{|y_{min} - y|}{y_{max} - y_{min}} \right)_y \tag{3.4}$$

Chapter 4

Results

In this chapter, the results for the optimization are exposed, whether parametric or topological. Furthermore, the FE loads and constraints tests made, as well as the results for the final optimized part are also presented. The verification tests on the optimization tool being used will be analysed and compared with already available studies in the field.

4.1 Problem Description

Before starting to use an optimization tool, it is of importance to know and to understand how it works. By this it is meant that one must have in mind what kind of constraints are present in the domain, whether they are space or material constraints, what kind of loads is it subjected to and what is its purpose, once it must be known how far can the optimization go and what are its admissible starting points. Of course, only by having the capacity to simulate the conditions to which the model is subjected in the best way possible one will able to successfully optimize the structure.

4.2 First Approach

As a first approach to the problem, a simpler body (but still similar) was chosen to be subjected to the optimization processes. This structure consists only in one antenna, once this will allow us to see the general effects of the studies on a similar body, minimizing time in computer processing. As mentioned in chapter 3, two kinds of optimization were performed, and a few different solutions of each are presented throughout this section.

4.2.1 Mesh Convergence

Given the fact that values like deformation, stress or strain tend to vary with the number of elements present on the mesh, the convergence studies allow retrieving the best results, as for sufficient number of elements these values tends to stabilized values. The present test will be divided in two main studies, where each depends on the number of layers present on the structure thickness: one with three layers

and another with five layers. Beginning with the three element layer, the study will be led by changing the size of each element, changing the number of elements present.

4.2.2 Parametric Results

In this subsection, the results for the primary parametric optimizations is exposed and analysed in the form of charts. This study consists in using the model, as well as its loads and constraints, as described in the end of the section 3.2.1 and illustrated in Fig. 3.8.

In the first analysis made, the only barrier imposed was σ_{max}. This stress was located on the corners of the back face of the antenna (Fig. 4.1), making perfect sense once this is the place that is constrained and in theory it would be where most stresses would concentrate. Taking into account the value of the maximum stress allowed for this material at the given temperature, a constraint in the study was defined in order to pick the best results for maximum stress bellow 195 MPa, i.e. the five results with the lowest values of stress would be picked.

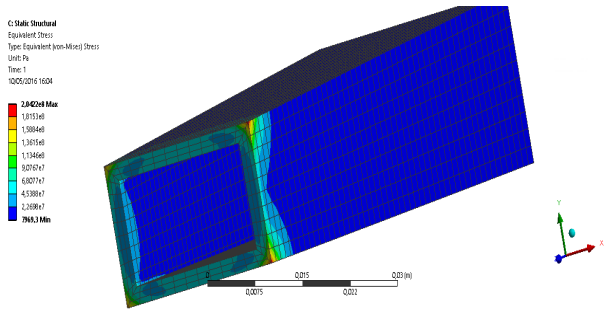

Figure 4.1: Stress concentration on the antenna

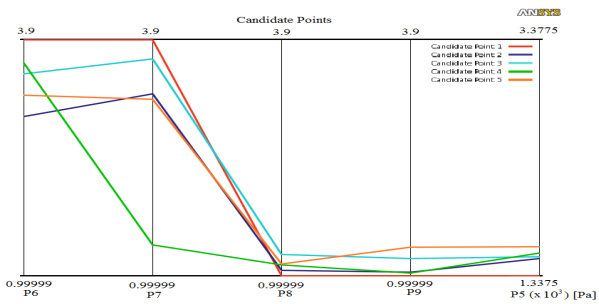

Figure 4.2: Resulting parameters for five best design points

In Fig. 4.2 one is able to see the five results for each of the five parameters defined, where the first two (P6 and P7) are representative of the thicknesses of the back of the structure, P8 and P9 represent the thicknesses of the front of the structure and P5 represents σ_{max}. From the chart, it is possible to see that the best case (line in red) relates to a design point where all the thickness parameters have limit values and as a result the maximum stress was of 137.4 MPa. This case presents a form where there's an increase of the rear vertical and horizontal thicknesses to a maximum of 3,9mm and where the remaining parameters decrease to a minimum of 1mm of thickness. It's a result that is coherent with

the idea that in order to compensate the stresses, more material may be needed and once the maximum stresses are located on the back of the antenna, it is there that more material should be included.

After performing a primary parametric optimization, illustrating the conjecture that more material would be beneficial in terms of the stress concentrations, further studies are performed with a more updated antenna model.

4.3 Verification

If the tests proposed to be made on the antenna are to be considered valid and well fundamented, a verification for the procedure implemented to use the software to that end must firstly be done.

This analysis is divided in three main groups, where it is initiated with a Steady State Thermal analysis, followed by a Static Structural in order to define the constraints and forces acting on the domain and finalizing with the topology optimization method, which gives us the final resulting antenna.

The same CAD design software that is used in designing the antenna is also used here (Solidworks), where the part is sketched with the exact same measures as in the already published results [45]. As also present in [45], a model with the dimensions 720 x 477 x 10 mm is built and a standard material present in ANSYS Workbench (Structural Steel with a Young's Modulus of E =200$\times$10^9 Gpa, a Poisson Ration ν =0,3 and a Thermal Condutivity k =60,5Wm$^-1$C$^-1$). In order to strengthen the results, the same FE mesh will be applied, where there are 60x30 elements in the surface, resulting in more viable numbers once the variables are maintained.

4.3.1 Verification for Thermostructural Analysis

The thermal loads are temperatures defined on each edge of the structure. The temperature chosen for the environment is ΔT$_{ref}$=22°C as well as for the initial temperature on each edge of the rectangular shape. Like in the paper [45], previously mentioned in this section, three different cases are generated, with the first having a ΔT=0°C, the second having ΔT=1°C and the last ΔT=4°C, where the only temperature that will change will be the one of the bottom edge of the shape, as seen in Fig. 4.3:

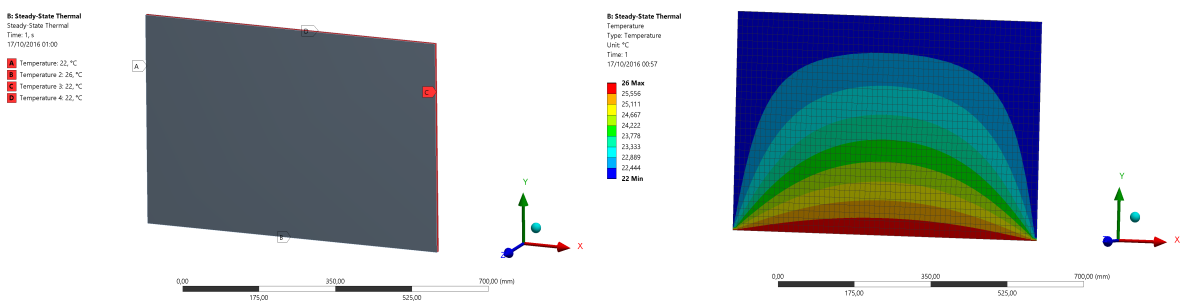

(a) Selected model edges

(b) Temperature distribution in the model.

Figure 4.3: Verification model thermal constraints.

After the thermal gradient is generated, it's time to define the constraints in the domain, where the part will be fixed and subjected to a descendant force. The structure will be clamped (fixed support) in

both lateral edges (parallel to axis y) and a force of 1000kg (F=9810 N, considering g=9,81 m/s^2) in the middle of the bottom edge, as illustrated in Fig. 4.4.

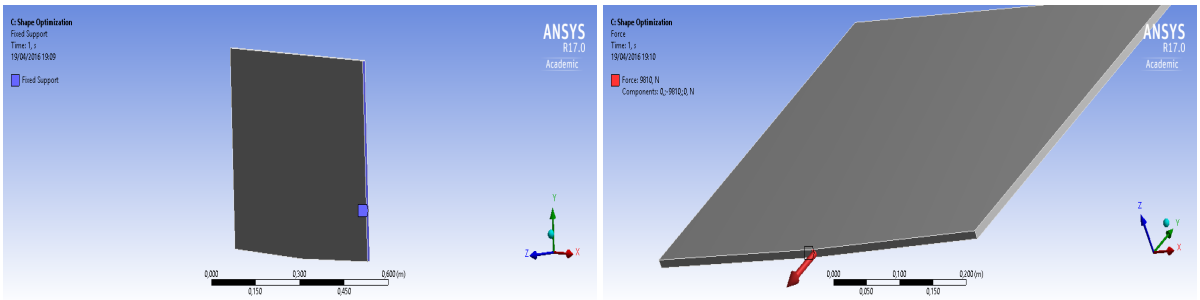

(a) Fixation locations of model.

(b) Force applied to the model.

Figure 4.4: Verification model for elastostatic analysis.

In order to validate the TO software used, three tests are made using a same model. These tests are compared to the literature results of TO applied in a thermally and static loaded structure, which is the case in this work (the antenna). Considering this, topology optimization by the SIMP method was applied to a rectangular shape subjected to thermal loads like in Fig. 4.5 [45].

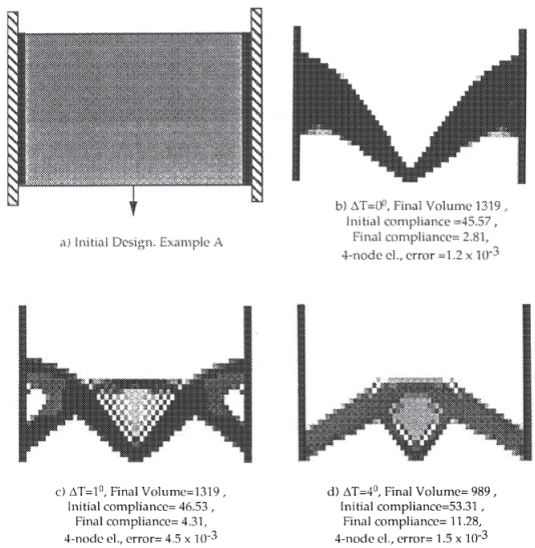

Figure 4.5: Topology Optimization using thermal loads in [45]

Having the literature results present for comparison, the topology optimization method (SIMP) using SO is applied to the already "stressed" model of Fig. 4.3 and Fig. 4.4. Here, a body subjected to a thermal gradient and a force is optimized in search for a stiffer structure through the Eqs. found in section 2.5.

Analysing the resulting geometries in Fig. 4.6, and having in mind that different tools were used when the data in the paper [45] was created, it can be stated the all the results are very similar to the correspondent previous result, which makes this a good method to apply in the analysis from now on. As it was not possible reproduce the exact same model as in [45], one has to compare the compliance results by looking at its variation in the beginning and in the end of the optimization process.

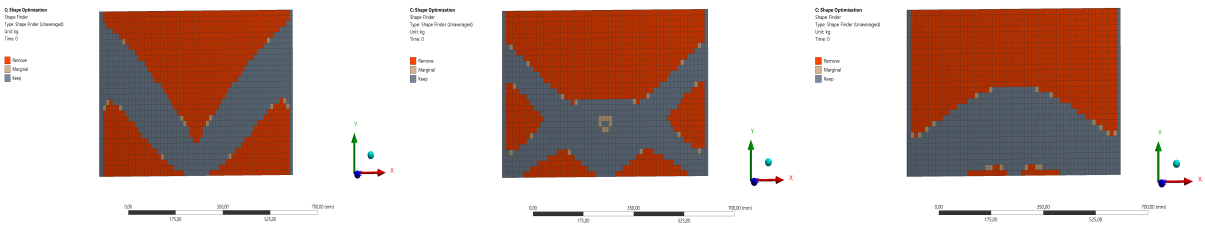

Figure 4.6: Topology optimization results for ΔT=0°, ΔT=1°, ΔT=4° from left to right.

4.3.2 Topology Optimization Results

Topology Optimization performed using the SO tool of ANSYS is a process that must be prepared with some care. For the given loads, temperature and displacement constraints applied to the body, the algorithm removes material from where it is not needed, increasing the stiffness of the remaining zones with material. If no constraint is imposed to the design, the algorithm can eliminate the material existing there, which gives origin to some impractical results like in Fig. 4.7.

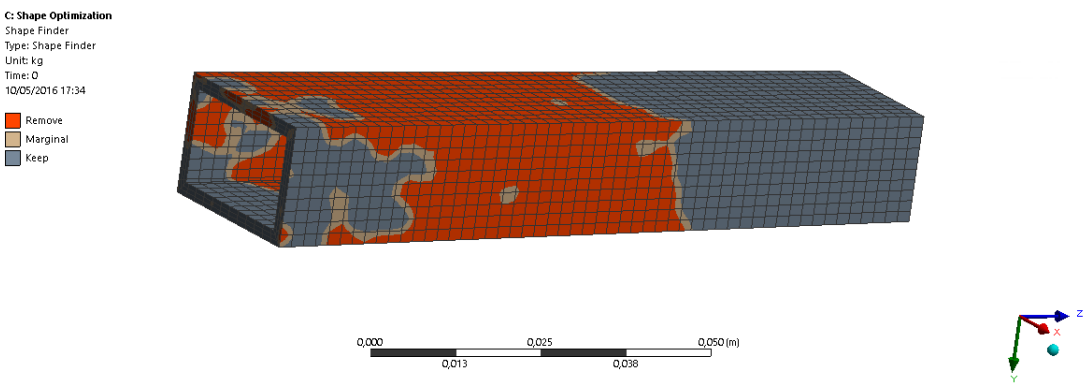

Figure 4.7: Resulting geometry from fixing the rear face of the structure

In Fig. 4.7 is illustrated the result of the antenna design mentioned in section 3.2.1 and already used in section 4.3.2 (Fig. 3.8 and Fig. 4.1, respectively) with the same loads and constraints. Furthermore, the structure was subjected to a volume constraint of 50%, i.e. the amount of volume that remains from the original body is 50%. The red coloured parts of the body are the ones where material has been removed. With this discontinuity, the desired part stops being one piece, to become two separate pieces, deviating from the initial purpose.

To evade this effect, additional constraints are added to the feature, with most of them consisting in fixed supports. This will create the idea that the structure will need material in that particular zone, which will circumvent the issue at cause.

As a first example of this new criteria, all the eight inner vertices will be defined as fixed supports, once material in the corners of the structure as been seen to be effective and necessary:

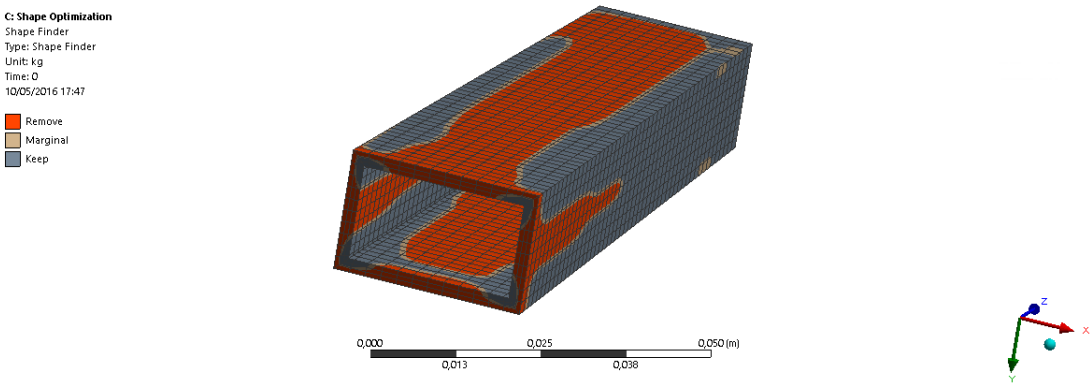

Figure 4.8: Resulting geometry from fixing the inner vertices

In an analog way to the case illustrated in Fig. 4.7, the same model, loads and constraints are applied in Fig. 4.8, as well as the volume constraint of 50%. Looking at the resulting geometry in Fig. 4.8 it is easy to remark that this is one only piece. This geometry reveals the need for more material on its lateral walls, exempting a great amount in the upper and bottom walls. If looked closely, it can be observed that more material is needed in the back, being in perfect harmony with previous results and only by adding fixed supports in the front material remained there.

Another interesting study would be to see what would happen if all the elements from the inner faces were kept. This can be achieved by defining the inner faces as fixed supports.

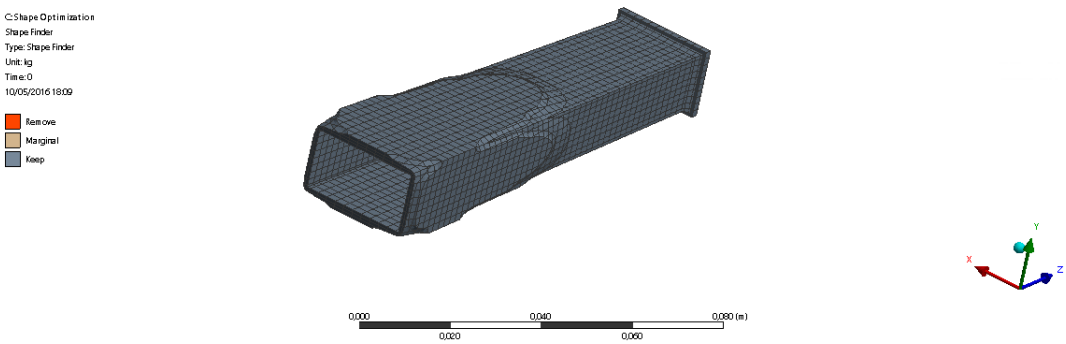

Figure 4.9: Resulting geometry from fixing the inner element layer

In Fig. 4.9 the inner layer of elements is maintained but it can be seen that all the material in the back of the structure would be retrieved if it wasn't for the constraints defined there. The amount of material that is left on the front is probably due to the high temperatures inflicting that zone, as well as for the deformations that it causes.

Looking at the results obtained in this section, although it was verified with literature results [45], one can state that, given the present work requirements, this TO software can not be used here. In the [45], the places where the structure is fixed coincidentally correspond to a area where material must not be removed and by that no problem was encountered. The fact that a fixed support must be set on a body component (face) in order to prevent the software to remove material from it, makes it unviable once it corrupts the true constraints that must be applied in the model.

4.4 Objectives

Since the main objective is to decrease T_{max}, as well as D_{max} in the antenna model, one must first identify how and where will these features occur. For that purpose, Steady Thermal and consequent Static Structural analyses were conducted on the model.

4.4.1 Thermal Analysis

As mentioned before in section 2.1, high temperatures can cause problems in the corrrect functioning of the antenna and for that reason a temperature study is made. For this study, as already mentioned in this section, a Steady Thermal study is performed in the model. As mentioned in section 3.4.1, the internal heat generation results described in the same section are illustrated in Fig. 4.10.

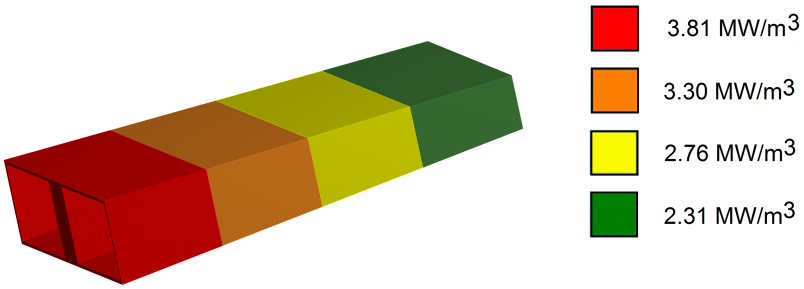

Figure 4.10: Nuclear heat load distribution on the antenna.

These results are part of the thermal analysis setting and the temperature distribution results are illustrated in Fig. 4.11.

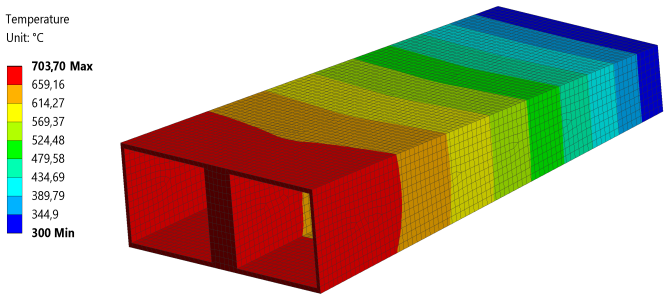

Figure 4.11: Distribution of T for the antenna without material coverage

In fig. 4.11 is possible to see not only the distribution of the temperature along the non-parametrized antenna model, but also where it has its maximum value T_{max}. This distribution is the effect of the loads and constraints defined in section 3.4.1, where temperatures, radiation and heat generation were set as the thermal analysis. As expected, this value is located in the front part of the antenna, once this is the first element in direct sight of the plasma resulting from the nuclear fusion process, reaching a temperature of around 704 °C. This temperature exceeds by far the desired limit of 600 °C mentioned in [41] which makes of extreme importance to lower these numbers in order to fulfil the project requirements.

However, this is not the only factor to have into account, as when looking again at Fig. 4.11, it's possible to see that not only T_{max} is surpassing the limit, but also another two fragments of the antenna have temperatures of 659,16°C and 614,27°C (when looking at the color division in Fig. 4.11). This behaviour leads to an increased necessity to decrease the model temperature also in its overall temperature.

4.4.2 Thermoelastic Analysis

Not only the temperatures affect the functioning of the antenna, also the displacements caused by the thermal effects and the gravitational acceleration lead to errors in the measurements made by the model and and material detrition. This is a problem that must also be minimized and a thermoelastic study is performed, where a Static Structural will be coupled to the previous Steady Thermal analysis, transferring the thermal load generated.

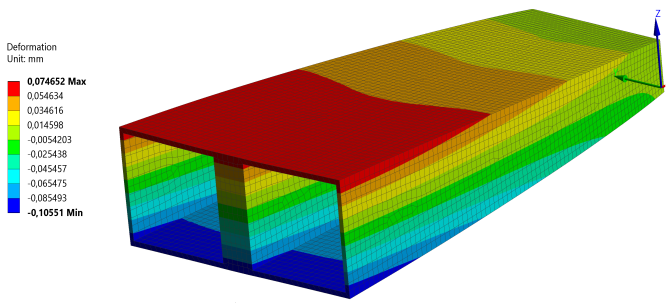

Figure 4.12: Distribution of D for the antenna without material coverage.

As illustrated in Fig. 4.12, D_{max} is located in the front part of the antenna. The model used, as in the previous section, is described in section 3.2.2 and all the loads and constraints are explained in section 3.4.2. This situation can be compared to the example of a clamped beam, where its unclamped extremity will be subjected to the act of gravity and reveal higher displacement values. As in the previous subsection, this area (front face of the antenna) is the first element in direct sight of the Plasma, which means that this is where the highest amount of energy acts and given the Eqs. present in section 2.2 2.2.

Another aspect to notice in the above figure is that in the downward direction the displacement is bigger than the upward direction. This phenomena happens once the only static load being applied in the model is the Earth Gravitational Acceleration, which has a direction parallel to the z axis present in Fig. 3.14.

As a result of the thermal expansions and action of gravity, D_{max} reaches a value of around 0,106 mm, which is a considerable number given the project requirements.

4.5 Design Optimization

Given the fact that the main priority of the work being developed is the minimization of the maximum temperature generated in the antenna, the design optimization must go in that same direction. It would

be a interesting option to use SIMP method of topology optimization to do so, but it has shown to be inefficient for that purpose given the constraints and non-removable material problems already explained in section 4.3.2.

Although this is a fairly know structural optimization tool, the nature of the present project doesn't allow TO to be used. Radiation, which represents the majority of the energy exchanges, reveals itself as an obstacle to this path given its surface to surface definition. When applying TO method to our model, as mentioned in section 3, the amount of new surfaces created is tremendous as for the view factors that come with it. This circumstance would demand a much more expensive computational process, which would only consume a proportional amount of precious time.

4.5.1 Temperature Parametric Results

As a result of the issues stated above in this section, the parametric study was picked as the successor method to improve the structure.

Looking at subsection 2.2.0.1, one would expect to obtain lower $\mathrm{T}_{\mathrm{max}}$ in the front of the antenna given the heat transfer process. With more material in the back of the body, an amount of the energy retained in the front of the antenna would migrate through conduction to the newly generated material in the back. If it sounds simpler, this process can be compared (in a way) with the osmotic process in Biology: once more material is added to the model, an osmotic pressure will be created, leading to the migration of water (in our case energy) to the place where exists deficit of it in order to generate a new equilibrium. Like in the process before, the existing surfaces in the antenna (including the new ones created) will not only receive energy through radiation, but will also emit, relieving also an amount of energy present in the body.

In order to verify how would the coverage mentioned in section 3.1 and illustrated in Fig. 3.4 acts on $\mathrm{T}_{\mathrm{max}}$, a parametric study was conducted varying both L_{c} and t_{c}:

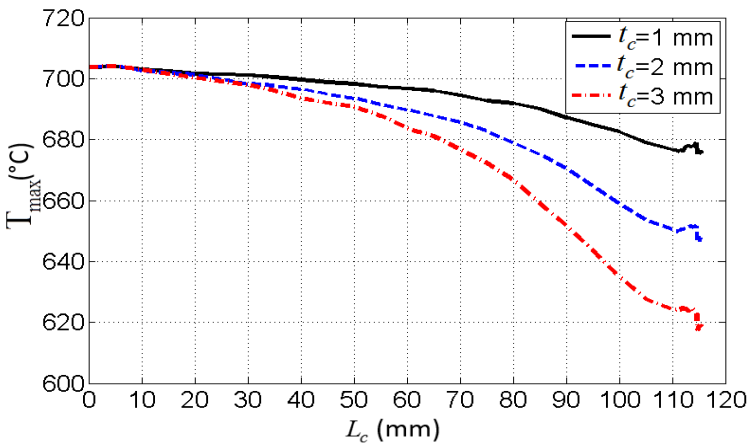

Figure 4.13: Parametric results for L_{c} and t_{c}

Analysing Fig. 4.13, where one can see the evolution of the coverage along the antenna (L_{c}) for three different thicknesses (t_{c}=1mm, t_{c}=2mm and t_{c}=3mm), it is possible to see the clear descending of

T_{max} values both with L_c and t_c increment. These results support the thesis endorsed previously in this subsection, that with more material the energy existing in the body would tend to scatter along the solid, decreasing T_{max}.

Furthermore, it is possible to see that there is a T_{max} reduction until a certain point nearly at the end of the antenna, from where the temperature starts to rise again. From this, one is able to find the L_c and t_c range of values where T_{max} will have its minimum point, i.e., have the greatest amount of material coverage possible, leaving a small part of the antenna uncovered.

4.5.2 Displacement Parametric Results

In this sub-chapter the behaviour of D_{max} towards the coverage will be studied. For that purpose, a parametric study was also conducted, in the same means as for T_{max} in the previous subsection. The idea of more material covering the rear part of the antenna induces the thought that it will create a stiffer structure which will allow less deformations.

As the Displacement is a very different entity from the Temperature, it is not expected to see a reproduction of the results for T_{max} here. If material is added to the model in a way that it covers most of its surfaces areas, or even all of its areas, it is not expected to see a D_{max} decrease, by the contrary, it's expected to see an increase of these values after a certain point. This can be easily explained by the fact that, besides the fact that more material can mean more thermal expansions, gravity is the only structural load being dealt with here. Hereupon, this means that the solid is only subjected to its own weight, i.e., the more heavier the structure gets (more material) after a certain point, the stiffest structure will no longer exist and the bigger the D_{max} is as in Fig. 4.14.

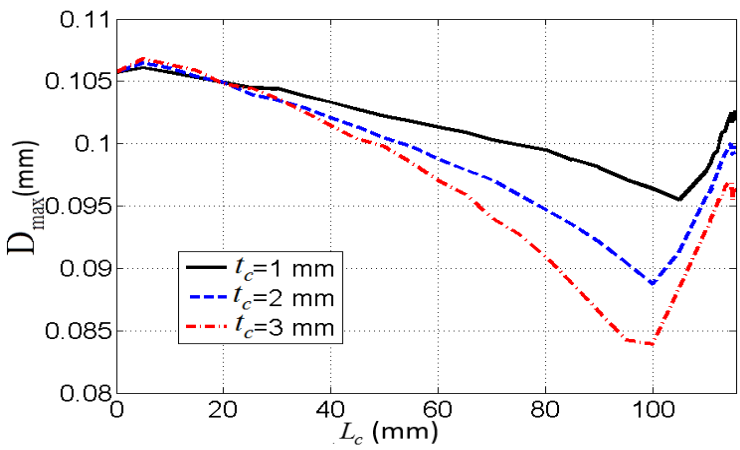

Figure 4.14: Parametric results of D_{max} for L_c and t_c variation.

By looking at Fig. 4.14 one can see that the results prove the comments done above. In the graphic where L_c and t_c vary in the same range of values as for the T study, a clear wane of D_{max} can be seen until it reaches a value of $L_c \simeq$ 100mm and after this point an increase to higher values occurs. This value supports the idea that the best compromise between the coverage and the stiffness of the structure will be located in a considerable distance from the full coverage of the antenna, in spite of the

fact that it will have a maximum thickness allowed t_c=3mm.However, in order to be sure on what is the real cause for the results presented in Fig. 4.14, some more studies should be made to exclude other possible causes.

With both parametric results for T and D, it is now possible to progress to a optimization algorithm capable of providing an optimum point in a fastest and more accurate way, once the parameters ranges of values have been reduced to a target scope.

4.6 Final Improvements in the Antenna

If aiming to achieve optimization through parametric studies, a primary study limiting the range of values of each parameters, as well as their relation, should be performed as it was done in the previous section. Having these results, it is now possible to proceed to the optimization algorithms as explained in the Methodology (chapter 3).

4.6.1 Reduction of maximum temperature in the antenna

Once it has already been shown that other optimization tools are inefficient to lower temperatures in the present project, ASO tool is chosen to perform the design optimization regarding temperature. In Methodology chapter it has been explained how does this tool works and which are the inputs needed to put it to work.

As in the parametric studies, the parameters used here are exactly the same, with the only difference residing in their range of values. From the parametric results, the value of t_c = 3mm and a range of 114 mm $\leq L_c \leq$ 115,4 mm are defined, where a small clearance has been given to the lower limit comparing to the value retrieved from subsection 4.6.1.

There are four main inputs that must be defined upon the optimization tool preparation: *Number of Initial Samples, Maximum Number of Evaluations, Convergence Tolerance* and *Maximum Number of Candidates*, that can be seen in Fig. 4.15.

Optimization	
Method Name	Adaptive Single-Objective
Number of Initial Samples	70
Maximum Number of Evaluations	300
Convergence Tolerance	1E-09
Maximum Number of Candidates	15

Figure 4.15: ASO preparation input definition.

Starting with the first, a number for the initial ”population” must be reasonable enough in order to have a sufficient amount of points that can include all the scope to be studied. It was chosen a number 70, which means that 70 initial design points will fill the space between L_c=110 and L_c=115,4. Looking at the second input, the value of 300 was defined as a safety measure in order to prevent the iterative process to stop before it reaches the convergence, which would make it inconclusive.

Regarding the Convergence Tolerance, as mentioned in section 4.2.1, the smaller this value is, the smaller is the difference between the first and the second best results, i.e. the more accurate the result

is, as the program only stops when there is a result convergence of that order.

For the final input, a reasonable number of candidates is chosen taking into account the number of design points that might be generated. The value of 15 is enough to see how the best designs are generated.

After inputs and parameters are defined, the only objective is set, which consists in minimize T_{max} that has also been set as a parameter in the Steady Thermal analysis.

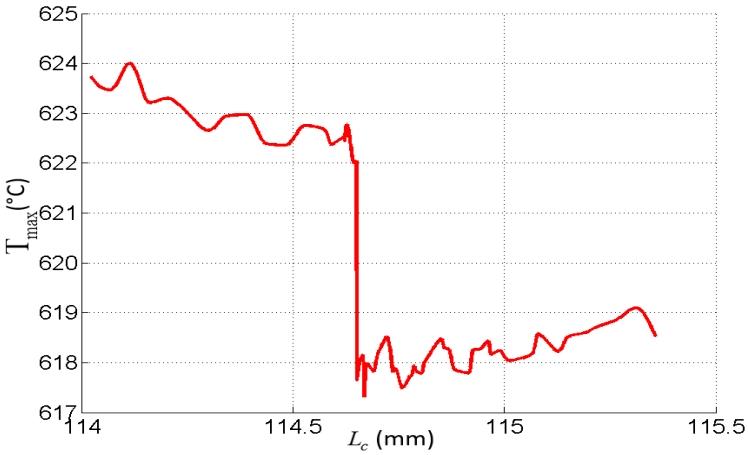

Figure 4.16: ASO results for L_{c} and T_{max}.

In Fig. 4.16 it is visible a similar efect to the one observed in the parametric studies, where a clear descent of T_{max} values is only interrupted when it reaches its minimum point (optimum) and is then followed by a rise until the maximum coverage is hit. From Fig. 4.16 it is possible to retrieve the best candidate, which is located in L_{c}=114,7mm and results in T_{max}=617,3°C. The decrease of T_{max} is perfectly visible, having reduction of 86,4°C, translating in a reduction of 12,3% from the original model. Note that the significant decrease in temperature near L_c =114,7 mm may be due to the fact that the plasma neutronic related heat leads extraction is at its maximum by conduction to the back of the antenna. Besides, the radiation gradient is practically the same.

Besides this, it is interesting to see, even if it was not set as an optimization objective, if the overall temperature of the model decreases. In order to achieve this, all the 141598 nodes temperature was extracted and their matching mean value has been calculated, where T_{mean}=500,5°C . This shows a clear decrease also in the mean temperature of the body, which expresses as a reduction of 56,2°C, i.e., a reduction of 10,1% comparing to the case where there is no coverage in the antenna (original).

Resembling to the case of T_{max}, also the T_{mean} decrease can be explained by the conduction process, where the amount of energy present in the antenna is scattered through the new structure. As this structure is bigger, it has more nodes, thus, better energy distribution through all nodes.

Although the results obtained are considered correct, another ASO optimization was operated on the model, as a way of acknowledging the correctness of this method. For that purpose, the range of values for both L_{c} and t_{c} was set to it maximum allowed, i.e., 0mm $\leq L_{\text{c}} \leq$ 115,4mm and 0mm $\leq t_{\text{c}} \leq$ 3mm. This means that the study will take place for every option available of coverage, depending on the program restrictions. In this case, the only modification regarding the previous ASO optimization was resided in

the *Maximum Number of Candidates*, which had to be bigger in order to try to reach all the spectrum of values, adopting a value of 100.

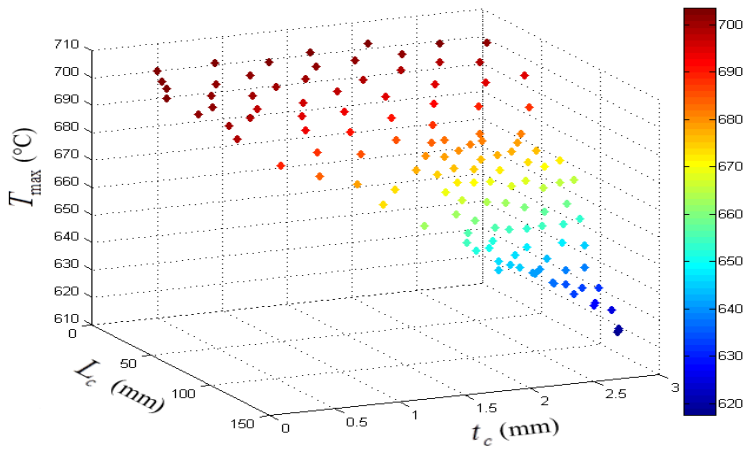

Figure 4.17: ASO 3D results for T_{max}, L_{c} and t_{c}.

Although through the graphic present in Fig. 4.17 it's not possible to see in a accurate way the best result, one can see the evolution towards the best candidate and that this will be located somewhere in t_{c}=3mm and between 110mm $\leq$ $L_{\text{c}}\leq$ 115,4mm, but though data analysis one obtains a value of L_{c}=114,7mm. This value validates the above results, as it is exactly the same, but at the cost of a much more time consuming computational process, which makes it unnecessary once the sensibility analysis (parametric) had already been made. Again, it may require more studies to be sure of what is involved.

Now, having the results for the optimum design for a minimum T_{max}, one is able to draw the antenna in its final stage, as seen in Fig. 4.18.

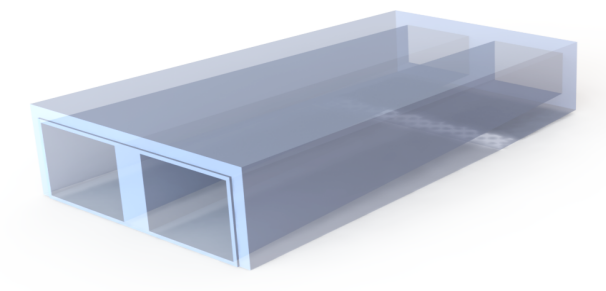

Figure 4.18: ASO geometry result for minimum T_{max}.

Knowing that the T_{max} if the coverage (with t_{c}=3mm) would be equal to $\approx$620°C, the gap visible between the coverage and the end of the antenna in Fig. 4.18, in spite of its relatively small dimension, translates in a difference of 0,44%. Despite the fact that it's a relatively small difference, a ΔT $\approx$3°C might actually be of some relevance regarding material properties and the main goal of the work developed was to find the optimum design, which has been found.

4.6.2 Multiple Optimization

Since the main priority of this project is to minimize temperatures, a study for the single optimization of D_{max} was not implemented as it would not have the same impact. Hence, in order to keep the path that has been travelled so far, a hybrid study is performed having as a mission the optimization of the structure concerning both T_{max} and D_{max}.

As discussed in section 3.5.2, the considered most suitable method to combine here both temperature and displacement is the AMO, which is able to execute two or more objectives. Given the dual objective nature of this optimization, in addition to the ASO case, two target parameters must now be defined: T_{max} and D_{max}.

Once again, the type optimization here being implemented uses the same variables used in the parametric studies, but, unlike the previous optimization, there is no mixed parameter work already done. Therefore, the user must have the insight to be able to choose an amplitude of values capable of representing the area where the mixed optimum point will be located. Looking at both "sensibility" studies, for the T_{max} case, a response should be placed somewhere between 110mm $\leq L_{\text{c}} \leq$ 115,4mm and t_{c}=3mm, while for the D_{max} case, the response should be placed somewhere between 90mm $\leq L_{\text{c}} \leq$ 110mm and t_{c}=3mm. So, a comprehensive spectrum of 90mm $\leq L_{\text{c}} \leq$ 115,4mm is defined, once it involves both required responses action zones, i.e. the spectrum must comprehend the ASO desired range of values and the AMO desired range of values, so a common range of values is used.

In a similar way to ASO optimization, also some inputs have to be set prior to solving the algorithm, which are: *Number of Initial Samples, Number of Samples Per Iteration, Maximum Alowed Pareto Percentage, Convergence Stability Percentage, Maximum Number of Iterations* and *Maximum Number of Candidates*, that can be seen in Fig. 4.19.

Optimization	
Method Name	Adaptive Multiple-Objective
Number of Initial Samples	100
Number of Samples Per Iteration	60
Maximum Allowable Pareto Percentage	70
Convergence Stability Percentage	1
Maximum Number of Iterations	100
Maximum Number of Candidates	15

Figure 4.19: AMO preparation input definition

Starting with the *Number of Initial Samples*, a number of 100 is chosen, given the demanding criteria as well as the considerable scope of possible design points. From here, the number of *Number of Samples Per Iteration* must not exceed the previous input, but must not be too high due to the consequent time that each iteration consumes.

Regarding the *Convergence Stability Percentage*, the values chosen, as for the ASO *Convergence Tolerance*, must be as low as possible in order to enable the optimization to function until it finds the optimum point. Once this feature is related to the difference between the two best candidates, if chosen a low value one does not have to worry about the program stopping before it encounters a optimum point.

About the *Maximum Number of Iterations*, in analog way to the previous input, has a resemblance

to what happened in ASO input *Maximum Number of Evaluations*, as this value must be high enough in order to prevent the program to stop before reaching its goal.

Finally, as in ASO, a number of points in *Maximum Number of Candidates* is defined in a way that the user can see how will the best designs be displayed.

After this step, since there are two different objectives and none of them must have bigger importance than the other, an importance defined as ”Default” is chosen for each one in order to guarantee this effect, as explained in section 2.5.2.3.

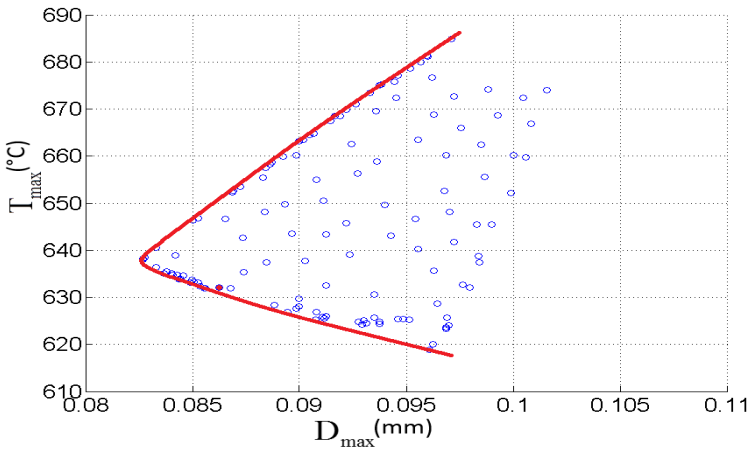

Figure 4.20: Pareto front obtained for L_c and t_c.

Fig. 4.20 illustrates the Pareto front obtained in the optimization, where the best point is indicated with a filled red circular dot. In this design point, located in L_c=102,8mm and t_c=3mm, a T_{max} of 631,9°C and D_{max} of 0,087mm are retrieved, meaning that a reduction of 10.2% (71,8°C) and 17.9% (0,019mm) in T_{max} and D_{max}, respectively. Besides this, employing the same method as for ASO, a value of 492,6°C is obtained for T_{mean} in all the 135914 present nodes, representing a reduction of 11,5% repecting T_{mean} for the initial antenna design (no coverage).

As for the ASO optimization, the results for temperatures retrieved show a clear reduction that can be explained with the conduction process in a bigger amount of material to where energy can migrate and ”relieve” the temperatures maximum values, as well as the overall temperature value of the body, resulting in the following geometry ilustrated in Fig. 4.21.

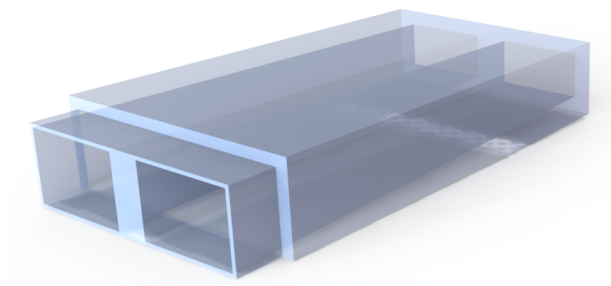

Figure 4.21: AMO geometry result for T_{max} and D_{max} minimization

Although the T_{max} acquired with this optimization exceeds the T_{max} value for full coverage in 1,92%, the results for D_{max} show a reduction of 35,6% regarding the result for full coverage of D_{max}=0,118mm.

To conclude this chapter, Table 4.1 is presented, where all the results concerning the the ASO and AMO optimizations compared to the initial state will be expressed.

Table 4.1: Initial and optimized results obtained by ASO and AMO.

						Decrease (%)		
	L_{c} (mm)	t_{c} (mm)	T_{max} (°C)	T_{mean} (°C)	D_{max} (mm)	T_{max}	T_{mean}	D_{max}
Initial	0	0	703.7	556.7	0.106	-	-	-
ASO	114.7	3	617.3	500.5	-	12.3	10.1	-
AMO	102.8	3	631.9	492.6	0.087	10.2	11.5	17.9

Chapter 5

Conclusions

In the present thesis is presented a study of design optimization methodologies for the antenna present in GAP 4 of the ITER PPR System. The first approach was supposed to be a topology optimization of the antenna aiming to decrease its T_{max} and T_{mean}. Although there are some promising studies in the area, whether in conduction [46] or even in radiation [47] problems (where it is mentioned that radiation boundary conditions can be readily recast mathematically in the form of a nonlinear convective boundary condition), they are still very embryonic and not available in commercial codes as far as the author knowledge. In the present case it would consume a significant amount of time, which was not available. Once the main objective of this work was to operate on a coverture of the antenna to minimize the maximum temperature and maximum displacement. In order to achieve that, a CAD model design was studied and parametrized to be later used in FEM analysis consisting in thermal and thermo elastic studies. This required the construction of the model from scratch in a way that all the model requirements (body inclinations and constant thickness) were respected as well as the engineering aspects, which led to a process of forward and backwards movements but ending up with a solid parametric design.

5.1 Achievements

The major achievements of the present work were the following:

- In a primary phase, parametric studies show that both T_{max} and D_{max} decrease with the addition of material until a certain point, i.e., both decrease with the increase of t_{c} and L_{c} until a optimum L_{c} is reached;
- A decrease of 12.3% and 10.1% was obtained in T_{max} and T_{mean}, respectively, with ASO method;
- A decrease of 10.2%, 11.5% and 17.9% was obtained on T_{max}, T_{mean} and D_{max}, respectively, with AMO method;

Regarding the results obtained for both T_{max} and T_{mean}, and if one additionally considers fatigue and creep phenomenas (not studied here) it is possible to affirm that the lifespan of the antenna is extended which translates into less maintenance and of course in a more resistant part. This is a crucial aspect

given the project characteristics, once reaching the component in question for maintenance or even swap purposes is of extreme difficulty.

As for the results obtained for D_{max}, the improvement obtained allows the improvement of the signal propagation and the data retrieved by the antenna to be more accurate, i.e., more accurate estimations for the plasma position are expected.

5.2 Future Work

As future work, it is suggested to continue this study exploring the existing space between the antenna and the blankets in order to verify the evolution of the results when adding more material. It would also be beneficial to apply different optimization techniques to the part, as the SIMP method of TO aiming to decrease D_{max} and study the applicability of this method respecting temperature.

Also, additional studies sould be made concerning the sudden change that occurs on the plots around L_c =110-115 mm.

Furthermore, it is suggested to apply similar design optimization methodologies to other PPR components.

Bibliography

[1] B. Briseghella, L. Fenu, C. Lan, E. Mazzarolo, and T. Zordan. Application of topological optimization to bridge design. *Journal of Bridge Engineering*, May 2012. doi:10.1061/(ASCE)BE.1943-5592.0000416.

[2] B. Lia, J. Hong, and Z. Liub. Stiffness design of machine tool structures by a biologically inspired topology optimization method. *International Journal of Machine Tools and Manufacture*, September 2014. doi:10.1016/j.ijmachtools.2014.03.005.

[3] D. Xiao, X. Liu, W. Du, J. Wang, and T. He. Application of topology optimization to design an electric bicycle main frame. *Struct Multidisc Optim*, May 2012. doi:10.1007/s00158-012-0803-7.

[4] M. P. Bendsøe and N. Kikuchi. Generating optimal topologies in structural design using a homogenization method. *Computer Methods in Applied Mechanics and Engineering 71*, March 1988.

[5] O. Sigmund. Design of material structures using topology optimization. *Ph.D. Thesis, Department of Solid Mechanics, Technical University of Denmark*, Oct. 1994.

[6] M. Bendsøe and O. Sigmund. *Topology Optimization - Theory, Methods, and Applications*. Springer, 2nd edition edition. DOI:10.1007/978-3-662-05086-6.

[7] L. Krog, A. Tucker, and G. Rollema. Application of topology, sizing and shape optimization methods to optimal design of aircraft components. *Proceedings of 3rd Altair UK Hyper- Works users conference*, 2002.

[8] M. Zhou, R. Fleury, Y. Shyy, H. Thomas, and J. Brennan. Progress in topology optimization with manufacturing constraints. *Proceedings of the 9th AIAA MDO conference AIAA-2002-4901*, 2002.

[9] M. Tomlin and J. Meyer. Topology optimization of an additive layer manufactured (alm) aerospace part. *The 7th Altair CAE technology conference*, 2011.

[10] J. Zhu, Y. Li, and Z. W.H. Topology optimization with shape preserving design. *Proceedings of 5th international conference on computational methods*, 2014.

[11] A. Remouchamps, M. Bruyneel, C. Fleury, and S. Grihon. Application of a bi-level scheme including topology optimization to the design of an aircraft pylon. *Struct Multidisc Optim*, 2011. doi:10.1007/s00158-011-0682-3.

[12] J. Eves, V. Toropov, H. Thompson, P. Gaskell, J. Doherty, and J. Harris. Topology optimization of aircraft with non-conventional configurationss. *8th World Congress on Structural and Multidisciplinary Optimization*, 2009.

[13] How nuclear fusion reactors work. `http://science.howstuffworks.com/fusion-reactor4.htm`, . Accessed on June 7th 2016.

[14] Iter, what is iter. `https://www.iter.org/mach`, . Accessed on August 16th 2016.

[15] P. Varela. A methodology for the development of discrete adjoint solvers using automatic differentiation tools. *ITER_D_SGCQ2S v2.0*, July 2016.

[16] P. B. Quental, H. Policarpo, R. Luís, and P. Varela. Thermal analysis of the in-vessel components of the iter plasma-position reflectometry,. *Review of Scientific Instruments*, 2016. doi:10.1063/1.4960493.

[17] F.p. incropera et al. john wiley and sons, inc, editor. introduction to heat transfer, 2011.

[18] Theory reference for the mechanical apdl and mechanical applications. ansys, version 12.1. april. 2009.

[19] R. Santos, H. Policarpo, B. Gonçalves, P. Varela, E. Nonbøl, E. B. Klinkby, B. Lauritzen, Y. Romanets, R. Luis, and P. Vaz. Material assessment for iter's collective thomson scattering first mirror. *Proceedings of Advancements in Nuclear Instrumentation Measurement Methods and their Applications*, 2015. DOI: 10.1109/ANIMMA.2015.7465646.

[20] L.-E. Lindgren. *From Weighted Residual Methods to Finite Element Methods*. 2009.

[21] J. Reddy. *An Introduction to the Finite Element Method*. 3rd edition, 2006.

[22] R. Cook, D. Malkus, M. Plesha, and R. Witt. *Concepts and Applications of Finite Element Analysis*. 4th edition edition, 2001.

[23] P. Abraços. Analysis and design improvement of a spacecraft thermal deflector. Master's thesis, Técnico Lisbon, 2015.

[24] J. Reddy. *Mechanics of Laminated Composite Plates and Shells: Theory and Analysis*. CRC Press, 2004.

[25] ANSYS Academic Research Help Manual, Release 17.0, 2016.

[26] G. Nikishkov. Introduction to the finite element method. *University of Aizu, Japan*. Lecture Notes.

[27] R. D. Cook, D. S. Malkus, M. E. Plesha, and R. J. Witt. Concepts and applications of finite element analysis. *John Willy & Sons, Inc.*, 2002.

[28] J. Arora. *Introduction to Optimum Design*. Elsevier, 2nd edition, 2004.

[29] O. Sigmund. Morphology-based black and white filters for topology optimization. *Structural and Multidisciplinary Optimization*, 2007.

[30] J. Zhu, W. Zhang, and L. Xia. Topology optimization in aircraft and aerospace structures design. *Arch Computat Methods Eng*, 2015.

[31] X. Zhou, Y. Ma, Y. Tu, and Y. Feng. Ensemble of surrogates for dual response surface modeling in robust parameter design. *Quality and reliability engineering international*, 2013.

[32] T. Jiang and X. Zhou. Estimation of actuarial quantities at fractional ages with kriging. *Communications in Statistics - Theory and Methods*, 2016.

[33] O. Exler and K. Schittkowski. A trust region sqp algorithm for mixed-integer nonlinear programming. *Optimization Letters*, 2007.

[34] O. Exler, T. Lehmann, and K. Schittkowski. Misqp: A fortran subroutine of a trust region sqp algorithm for mixed-integer nonlinear programming - user's guide. *Report, Department of Computer Science, University of Bayreuth*, 2012.

[35] M. D. McKay, R. J. Beckman, and W. J. Conover. A comparison of three methods for selecting values of input variables in the analysis of output from a computer code. *Technometrics, Vol. 21*, May 1979.

[36] O. Exler, K. Schittkowski, and T. Lehmann. A comparative study of numerical algorithms for nonlinear and nonconvex mixed-integer optimization. *Mathematical Programming Computation, Vol. 1*, 2012.

[37] C. Coello, D. Van Veldhuizen, and G. Lamont. *Evolutionary Algorithms for Solving Multi-Objective Problems*. Genetic Algorithms and Evolutionary Computation. Springer US, 2013. ISBN 9781475751840. URL `https://books.google.pt/books?id=VmnTBwAAQBAJ`.

[38] Ansys DesignXplorer User's Guide v17, 2016. `http://148.204.81.206/Ansys/150/Design%20Exploration%20Users%20Guide.pdf`.

[39] H. Policarpo, N. Velez, P. B. Quental, R. Moutinho, R. Luís, and M. M. Neves. Optimum design of the iter in-vessel plasma-position reflectometry antenna. September 2016.

[40] A. Reyes. *Beginner's Guide to SolidWorks 2014 - Level I*. SDC Publications, 2014. ISBN 1585038415.

[41] Appendix A. Materials design limit data. *ITER_D_222RLN*, January 2013.

[42] C. Vacas. 55.F3 – PPR: Load Specification for In-Vessel components. *ITER_D_9QWLQ8*, January 2015.

[43] G. W. McKinney, F. B. Brown, and et al. Mcnp 6.1.1 new features demonstrated. *IEEE 2014 Nuclear Science Symposium, Seattle*, November 2014.

[44] A. Silva, H. Policarpo, and P. Varela. Assessment of stray-radiation protection needs for the ppr in-vessel components. *F4E_D_24LLE8*, March 2016.

[45] H. Rodrigues and P. Fernandes. Topology optimal design of thermoelastic structures using a homogenization method. *Control and Cybernetics, Vol.23*, 1994.

[46] K. Liu and A. Tovar. An effcient 3d topology optimization code written in matlab. *Struct Multidisc Optim*, 2014. doi:10.1007/s00158-014-1107-x.

[47] T. Bruns. Topology optimization of convection-dominated, steady-state heat transfer problems. *International Journal of Heat and Mass Transfer*, July 2007.

Chapter 6

Appendix A

This appendix contains information regarding the material properties of TYPE 316L (N)-IG Stainless Steel and their variation with temperature present in [41].

Element	Reference grade: 316L(N)-IG	
	min	max
C		0.030
Mn	1.60	2.00
Si		0.50
P		0.025
S		0.010
Cr	17.00	18.00
Ni	12.00	12.50
Mo	2.30	2.70
Ti Ta +Nb * Nb *		0.10 0.15 0.10 (0.01)
Ta*		0.01
Cu		0.3
B **		0.0010-0.0020
Co *		0.05
N	0.060	0.080

Figure 6.1: Chemical composition (in wt. %) of type 316L (N)-IG stainless steel.

T, °C	20	50	100	150	200	250	300	350	400	450	500
α_m, 10^{-6}/K	15.3	15.5	15.9	16.2	16.6	16.9	17.2	17.5	17.8	18.0	18.3
α_i, 10^{-6}/K	15.3	15.7	16.5	17.1	17.8	18.3	18.9	19.3	19.8	20.1	20.5

T, °C	550	600	650	700	750	800	850	900	950	1000
α_m, 10^{-6}/K	18.5	18.7	18.9	19.0	19.2	19.3	19.5	19.6	19.7	19.7
α_i, 10^{-6}/K	20.7	21.0	21.1	21.3	21.3	21.4	21.3	21.3		

Figure 6.2: Mean α_m (reference temperature - 20°C) and instantaneous α_i coefficient of coefficients of linear thermal expansion of type 316L (N)-IG stainless steel.

T, °C	20	100	150	200	250	300	350	400	450	500	550	600	650	700
E,GPa	200	193	189	185	180	176	172	168	164	159	155	151	147	142

Figure 6.3: Values of Young's modulus from room temperature to 700°C of type 316L (N)-IG stainless steel.

T, °C	20	50	100	150	200	250	300	350	400	450	500
ρ, kg/m^3	7930	7919	7899	7879	7858	7837	7815	7793	7770	7747	7724

T, °C	550	600	650	700	750	800					
ρ, kg/m^3	7701	7677	7654	7630	7606	7582					

Figure 6.4: Values of density from room temperature to 800°C of type 316L (N)-IG stainless steel.

T, °C	20	50	100	150	200	250	300	350	400	450	500
λ, W/(m K)	14.28	14.73	15.48	16.23	16.98	17.74	18.49	19.24	19.99	20.74	21.49

T, °C	550	600	650	700	750	800
λ, W/(m K)	22.24	22.99	23.74	24.49	25.25	26.00

Figure 6.5: Values of thermal conductivity from room temperature to 800°C of type 316L (N)-IG stainless steel.

Temperature, °C	20	50	100	150	200	250	300	350	400	450	500
Specific Heat, J/(kg K)	472	485	501	512	522	530	538	546	556	567	578

Figure 6.6: Values of specific heat from room temperature to 500°C of type 316L (N)-IG stainless steel.